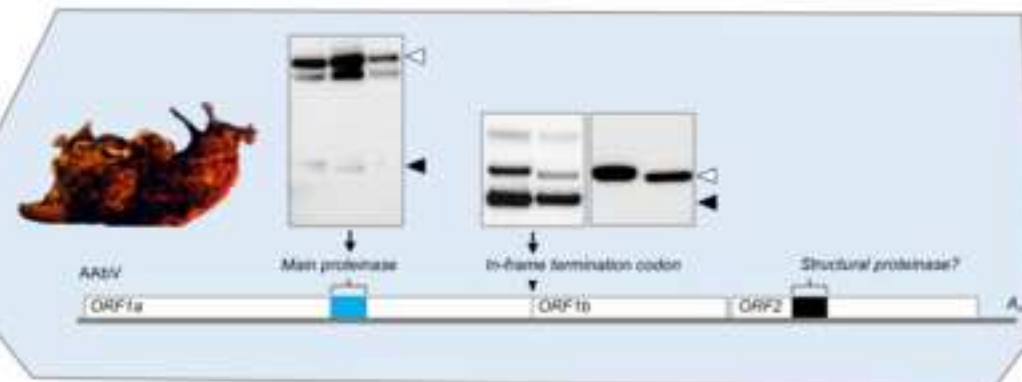
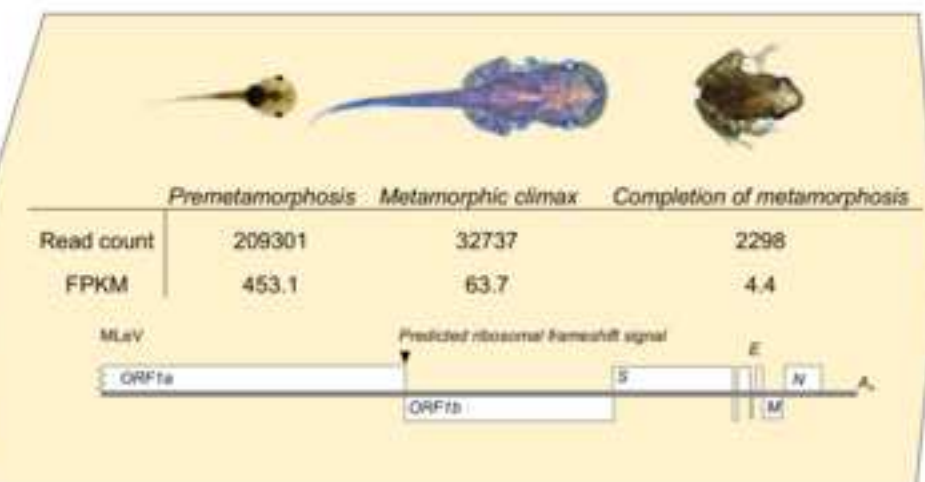
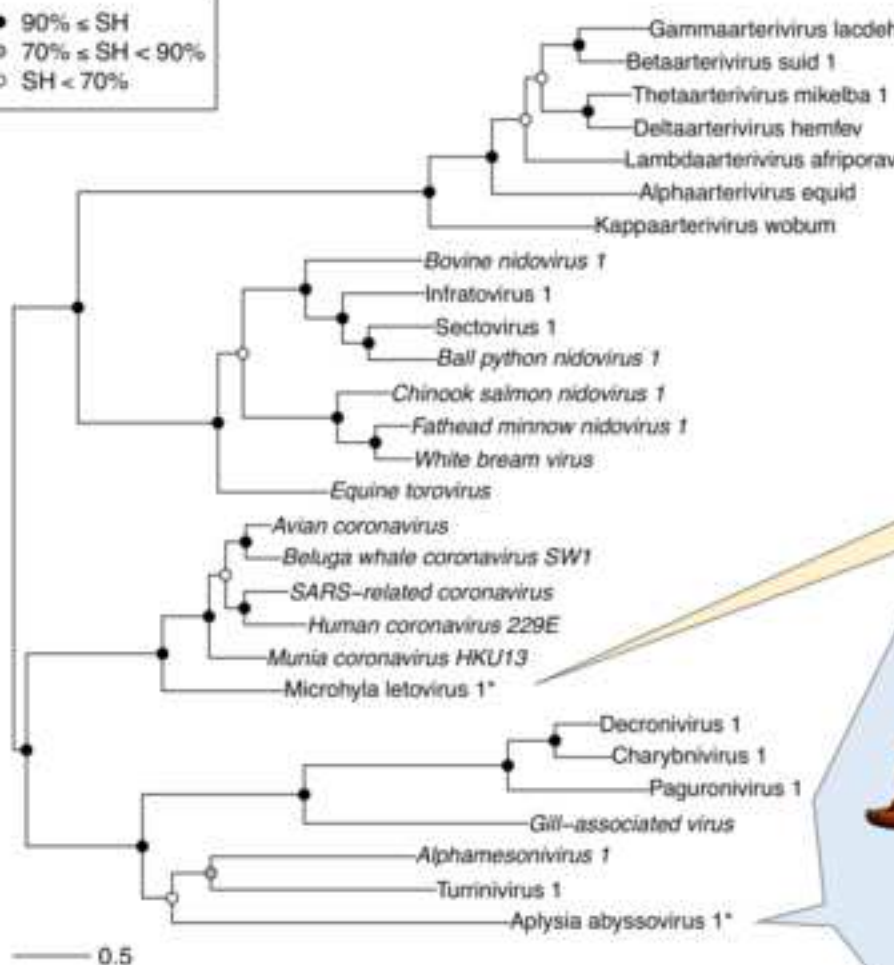


Graphical Abstract

- 90% ≤ SH
- 70% ≤ SH < 90%
- SH < 70%



1 **Title:** Description and initial characterization of metatranscriptomic nidovirus-like
2 genomes from the proposed new family Abyssviridae, and from a sister group to
3 the *Coronavirinae*, the proposed genus Alphaletovirus
4
5

6
7 **Authors:** Khulud Bukhari¹, Geraldine Mulley¹, Anastasia A. Gulyaeva², Lanying
8 Zhao³, Guocheng Shu³, Jianping Jiang³, Benjamin W. Neuman^{4,5}
9
10
11

12 **Affiliations**
13
14 ¹University of Reading, Reading, UK
15
16 ²Dept. Medical Microbiology, Leiden University Medical Center, Leiden, Netherlands
17
18 ³Chengdu Institute of Biology, Chinese Academy of Science, Chengdu, China
19
20 ⁴Texas A&M University-Texarkana, 7101 University Ave, Texarkana, TX 75503
21
22 ⁵Address correspondence to bneuman@tamut.edu
23
24

25 **Word count:** 5956 total, 135 abstract
26
27

28 **Abstract**
29
30 Transcriptomics has the potential to discover new RNA virus genomes by
31 sequencing total intracellular RNA pools. In this study, we have searched publicly
32 available transcriptomes for sequences similar to viruses of the *Nidovirales* order.
33
34 We report two potential nidovirus genomes, a highly divergent 35.9 kb likely
35 complete genome from the California sea hare *Aplysia californica*, which we assign
36 to a nidovirus named *Aplysia* abyssovirus 1 (AAbV), and a coronavirus-like 22.3 kb
37 partial genome from the ornamented pygmy frog *Microhyla fissipes*, which we assign
38 to a nidovirus named *Microhyla* alphaletovirus 1 (MLeV). AAbV was shown to
39 encode a functional main proteinase, and a translational readthrough signal.
40
41 Phylogenetic analysis suggested that AAbV represents a new family, proposed here
42 as Abyssviridae. MLeV represents a sister group to the other known
43 coronaviruses. The importance of MLeV and AAbV for understanding nidovirus
44 evolution, and the origin of terrestrial nidoviruses are discussed.
45
46
47
48
49
50
51
52
53
54
55
56
57
58
59
60
61
62
63
64
65

31
32 **Keywords:** Nidovirales; transcriptome; virus discovery; proteinase; protease; protein
33 expression; translation; readthrough
34

35 **Introduction**

1 36 Until recently, discovery of new RNA viruses proceeded slowly in a mostly
2 37 hypothesis-driven manner while searching for an agent of a disease, and using
3 38 antibody cross-reactivity or enough conserved motifs for successful amplification by
4 39 reverse transcriptase polymerase chain reaction. With improvements in RNA
5 40 transcriptome sequencing and homology-based search methods, it is now possible
6 41 to capture the complete infecting RNA virome of an organism by deep-sequencing
7 42 total intracellular RNA pools (Miranda et al., 2016; Shi et al., 2018, 2016).

14 43
15
16 44 The new sequencing methods have brought a great change to the *Nidovirales*, an
17 45 order that includes viruses with complex replicase polyproteins and the largest
18 46 known RNA genomes (Lauber et al., 2013). This order previously contained four
19 47 family-level groups, the *Coronaviridae* which infect birds and mammals including
20 48 humans, the *Arteriviridae* which infect non-human mammals, the *Mesoniviridae*
21 49 which infect arthropods, and the *Roniviridae* which infect crustaceans (Lauber et al.,
22 50 2013). However, recent papers (Lauck et al., 2015; O'Dea et al., 2016; Saberi et al.,
23 51 2018; Shi et al., 2018, 2016; Tokarz et al., 2015; Vasilakis et al., 2014; Wahl-Jensen
24 52 et al., 2016) and our results (see below) have added to within-family diversity and
25 53 revealed several highly divergent nido-like viruses which the *Nidovirales* Study
26 54 Group proposed, pending ICTV ratification, to form four new virus families within the
27 55 *Nidovirales* (Gorbalenya et al., 2017a).

38 56
39
40 57 In this report we describe the discovery and characterization of one of the
41 58 nidoviruses prototyping a new family along with another putative nidovirus. We used
42 59 BLAST searches to scan the publicly available transcriptomes and expressed
43 60 sequence tag libraries available at the US National Center for Biotechnology
44 61 Information, and revealed two novel nido-like virus sequences from the frog
45 62 *Microhyla fissipes* developmental transcriptome (Zhao et al., 2016) and from several
46 63 transcriptome studies dealing with the marine gastropod *Aplysia californica* (Fiedler
47 64 et al., 2010; Heyland et al., 2011; Moroz et al., 2006). We describe the
48 65 bioinformatics of the new virus-like sequences, and demonstrate that the *Aplysia*
49 66 virus-like sequence encodes a functional proteinase, and a translational termination-
50 67 suppression signal. Implications for nidovirus evolution and the origin of nidovirus
51 68 structural proteins are discussed.

69
1 70 **Results**
2
3
4 **Virus Discovery**

5 72 Recent studies have identified a wide variety of virus-like sequences in intracellular
6 RNA pools, but few new members of the *Nidovirales* have been reported compared
7 to groups such as the *Picornavirales*. In order to determine whether additional
8 lineages of nido-like viruses might be present, tBLASTn (Altschul et al., 1990) was
9 used to search the transcriptome shotgun assembly (TSA) and expressed sequence
10 tag (EST) databases for sequences encoding proteins similar to the main proteinase
11 (M^{pro}), polymerase and helicase, or complete pp1b regions of the nidovirus strains
12 used to search the transcriptome shotgun assembly (TSA) and expressed sequence
13 tag (EST) databases for sequences encoding proteins similar to the main proteinase
14 (M^{pro}), polymerase and helicase, or complete pp1b regions of the nidovirus strains
15 used to search the transcriptome shotgun assembly (TSA) and expressed sequence
16 tag (EST) databases for sequences encoding proteins similar to the main proteinase
17 (M^{pro}), polymerase and helicase, or complete pp1b regions of the nidovirus strains
18 Infectious bronchitis virus, Gill-associated virus, White bream virus, Cavally virus and
19 Wobbly possum disease virus. The tBLASTn results were checked by using
20 BLASTx to compare each result to the non-redundant protein database, and results
21 that matched back to any member of the Nidovirales were selected for further
22 analysis. This led to the discovery of a 35.9 kb transcript and 243 other fragments
23 from the California sea hare, *Aplysia californica*, and a 22.3 kb transcript from
24 *Microhyla fissipes*, known as the ornamented pygmy frog. Putative virus transcripts
25 were then compared to DNA sequences from the same organisms by nucleotide
26 BLAST, and no evidence of either virus was found. Together, these tests suggest
27 that both nidovirus-like transcripts most likely come from RNA viruses associated
28 with host transcriptomes.

38 90
39
40 91 **Phylogenetic analysis**
41
42 Phylogenetic analysis was performed by IQ Tree 1.5.5 (Nguyen et al., 2015) using
43 five protein domains universally conserved in known and proposed nidoviruses plus
44 the virus-like sequences described in this study (see below). The produced
45 maximum-likelihood tree was mid-point rooted to reveal two strongly-supported
46 super-clades, consisting of four strongly-supported major clades corresponding to
47 arteri-like viruses, toro-like viruses, corona-like viruses, and invertebrate nidoviruses
48 (Fig. 1). A Bayesian rooted tree (not shown) was also constructed using the same
49 viral sequences, and it yielded the same four major clades, but with weaker support
50 values on some branches and a basal position of the arteri-like major clade.
51
52 Together these results suggest that the novel virus-like sequences likely represent
53 distantly related members of the *Nidovirales*, but the tree branch uncertainty also

103 demonstrates the limitations of these phylogenetic approaches in dealing with the
104 extreme diversity of the sparsely sampled nido-like viruses.

105
106 The virus-like sequence from *Aplysia californica* formed a relatively long and
107 moderately supported branch that clustered with other invertebrate nidoviruses,
108 forming a sister group to a clade consisting of the *Mesoniviridae* and a recently
109 discovered nidovirus from the marine snail *Turritella*, TurrNV. The virus-like
110 sequence from *Microhyla fissipes* clustered with strong support as a sister group to
111 the known *Coronavirinae*. We named these putative viruses *Aplysia abyssovirus*
112 (AAbV) and *Microhyla letovirus* (MLeV), respectively.

113
114 While we were expressing viral proteins to biologically validate the new sequences
115 and preparing this manuscript, a second manuscript appeared on BioRxiv (Debat,
116 2018) from Humberto Debat who was describing the same *Aplysia* virus from the
117 same source material, posted April 24th 2018, where it is called *Aplysia californica*
118 nido-like virus. That report covers the tissue tropism and age-dependent prevalence
119 of the *Aplysia* virus thoroughly, so in this manuscript we will focus on bioinformatics
120 analysis and biological validation of this virus. It is our opinion that the name *Aplysia*
121 *californica* nido-like virus should be regarded as an alternate name to *Aplysia*
122 abyssovirus.

123 124 **Naming and Etymology**

125 After assigning AAbV and MLeV to nidoviruses by the above bioinformatics analysis,
126 the genome sequences were submitted to the Nidovirus Study Group (NSG) of the
127 International Committee on the Taxonomy of Viruses (ICTV) for their accommodation
128 in the nidovirus taxonomy; BN, senior author of this manuscript, is a member of the
129 NSG and AAG assisted NSG with analysis of these viruses. Classification of these
130 and other viruses were described in several taxonomic proposals that were made
131 publicly available in the pending proposals section of ICTV on June 23rd 2017,
132 revised on November 26th 2017(Gorbalenya et al., 2017b, 2017a; Ziebuhr et al.,
133 2017) and August 12, 2018. They were approved by the ICTV Executive Committee
134 in July 2018 and will be placed for ratification by ICTV in 2018. Throughout this
135 report, we will follow the taxa naming and taxonomy from the pending ICTV
136 taxonomic proposals cited above, which we interpret to establish priority in

137 discovering and naming these viruses and establishing the respective taxa.

138
139 The etymology of the name abyssovirus is from the word abyss, a reference to the
140 aquatic environment where *Aplysia* lives, to the Sumerian god of watery depths
141 Abzu, and to its discovery in an RNA transcriptome obtained by “deep” sequencing
142 technology. Based on relatively low amino acid identity to the other families in the
143 *Nidovirales*, it is our opinion that AAbV prototypes a new nidovirus family, which was
144 confirmed in the analysis described in the pending proposal. The NSG has also
145 accepted our proposal to name the new family *Abyssoviridae*, the new genus
146 *Alphaabyssovirus* and the new species *Aplysia abyssovirus* 1.

147
148 The etymology of the name letovirus is in reference to the source of the virus in
149 frogs, and their connection to the mythological Leto, daughter of the titans Coeus
150 and Phoebe. In the story, Leto turned some inhospitable peasants into frogs after
151 they stirred up the mud at the bottom of a pool so that she could not drink from it.
152 Based on the low sequence identity but high conservation of domains found in the
153 *Coronavirinae*, it is our opinion that MLeV is a member of a sister group to all known
154 coronaviruses, but still within the *Coronavirinae*. Based on our input, the NGS named
155 the new genus *Alphaletovirus* in the pending proposal.

156
157 **AAbV Genome and subgenome sequences and their potential expression**

158 The host of AAbV is shown in Fig. 2A. The virus was recovered from a variety of
159 adult tissues, and from several developmental stages of the host organism, as
160 described elsewhere (Debat, 2018). Fragments of AAbV were detected in 9 TSA and
161 9 EST databases, compiled over several years by three labs working in Florida and
162 the UK (Fig. 2B-C).

163
164 The AAbV genome is represented in its longest and most complete available form by
165 the transcriptome shotgun assembly sequence GBBW01007738 which represents a
166 reverse-complementary genomic sequence. Remarkably, the organization of the
167 AAbV genome has several features typical for viruses of the *Alphavirus* genus of the
168 *Togaviridae* family (King et al., 2012) that could be contrasted with those conserved
169 in the nidoviruses. They include: a) two in-frame open reading frames (ORFs;
170 ORF1a and ORF1b) of the replicase gene that are separated by a stop codon rather

171 than overlapping and including a nidovirus-like ribosomal frameshift signal in the
172 overlap, and b) a single structural polyprotein gene (ORF2) rather than several ORFs
173 encoding structural proteins. The 35913 nt long AAbV genome has a 74 nt 5'-
174 untranslated region, a 964 nt 3'-untranslated region, and a short poly-A tail (Fig. 2D).
175 Despite these alphavirus-like features, BLASTx analysis confirmed that the AAbV
176 replicase polyprotein clusters with the *Nidovirales*, as depicted in Fig. 1. Each part of
177 the genome is represented in 3-20 independent sequences from the TSA and EST
178 databases available at www.ncbi.nlm.nih.gov as of November 26th 2017 (Fig. 2E-F).
179 The AAbV genome (Fig. 3A) is the second-largest currently reported RNA virus
180 genome, behind a new 41.1 kb planarian nidovirus described in a BioRxiv
181 manuscript (Saberi et al., 2018).

182
183 The sequence of the genomic 5'-terminus is supported by the five assemblies
184 (GBBW01007738, GAZL01021275, GBDA01037198, GBCZ01030948, and
185 GBCZ01030949) that end within one nucleotide of each other. The EST sequence
186 EB188990 contains the same sequence with an additional 5'-GGCTCGAG-3' that
187 may represent part of the 5'-terminal region missing from GBBW01007738.
188 However, we prefer to side with the preponderance of sequence data and consider
189 GBBW01007738 the most complete AAbV genome available until further biological
190 evidence emerges.

191
192 The sequence of the 3'-terminus is supported by 6 TSA sequence assemblies and 1
193 EST sequence that all end within one nucleotide of each other. Every part of the
194 genome is represented in at least three TSA sequence assemblies. Genome
195 coverage is more abundant at the 3'-end, which could be evidence of 3'-coterminal
196 subgenomic RNA species, or could be a result of the method used to prepare cDNA.

197
198 Genetic variation among these sequences is as follows. There are four short EST
199 sequences which appear to join different discontinuous regions of the genome
200 together, but the joins occur at different positions in the middle of genes and cannot
201 be explained by nidovirus-like discontinuous transcription. These oddly joined
202 sequence fragments likely represent either defective RNA species (Furuya et al.,
203 1993), or artifacts of the EST preparation process. Two sequence assemblies
204 differed from the others, with A replacing G at nucleotide 1627, and in another

205 assembly A replacing the consensus G at position 28005, both of which could be
1 attributed to natural mutations or the actions of host cytidine deaminase on the viral
2 minus strand. There is also some variation in the preserved poly-A tail sequences,
3 presumably from the difficulty of accurately reading long stretches of a single
4 nucleotide.
5
6
7
8
9 210
10
11 211 In order to test whether there was support for AAbV subgenomic RNA species in the
12 raw sequence data, individual sequence reads were mapped to the AAbV genome
13 using Bowtie 2.3.4.1(Langmead and Salzberg, 2012) and SAMtools 1.9(Li et al.,
14 2009). There was no a noticeable change in read depth at the junction between
15 ORF1a and ORF1b, but there was a sudden increase of about seven-fold in read
16 depth immediately before the start of ORF2 (Fig. 3B), suggesting that ORF2 may be
17 expressed from a subgenomic mRNA produced in relative abundance compared to
18 the genomic RNA, as would be expected for a member of the *Nidovirales*.
19
20 219 Numerous low-frequency AAbV sequence variants were identified in the raw
21 sequence data, but none were consistent across all datasets, and no indels were
22 consistently present within 1000 nucleotides of the start of ORF2. This was
23 interpreted to indicate that either the viral subgenomic mRNA did not contain the
24 expected nidovirus-like leader-body structure, or that any potential 5'-terminal leader
25 sequences were not captured in the raw data.
26
27
28
29
30
31
32
33
34
35
36 225
37
38 226 Nidoviruses express their structural and accessory proteins via a set of 3'-coterminal
39 nested subgenomic RNAs, which are produced by discontinuous transcription on the
40 genomic template. In this process, the polymerase is thought to pause at
41 transcription-regulatory sequences located upstream of each gene, occasionally
42 resulting in a template switch to homologous transcription-regulatory sequence in the
43 viral 5'-untranslated region to produce negative-stranded RNAs of subgenomic size
44 (Sola et al., 2015). The longest sequence match between the 5'-untranslated region
45 and intergenic sequence of AAbV is shown in Fig. 3C. It consists of six of eight
46 identical nucleotides, which could form eight base pairs with a reverse-
47 complementary viral minus strand due to the possibility of both A-U and G-U wobble
48 base pairing. However, none of the available TSA or EST sequences showed direct
49 evidence of a subgenomic RNA species, such as a consistently-spliced transcript, or
50 a large number of sequence reads that stop at the putative transcription-regulatory
51
52
53
54
55
56
57
58
59
60
61
62
63
64
65

239 sequence. This sequence AAACGATG or AAACGGTA needs to be investigated
1 further to determine whether it functions as a transcription-regulatory sequence for
2 viral subgenomic RNA production.
3
4
5

242
6
7 Together these data suggest that the AAbV genome is reasonably complete, robust,
8 and represents a novel and exceptionally large nido-like virus. It has the unusual
9 genome organization which is nonetheless consistent with the canonical nidovirus
10 features of large replicase polyproteins 1a and 1ab, pp1a and pp1ab, respectively.
11
12 They are expressed via a translational readthrough rather than frameshift
13 mechanism, while potential structural protein genes are presumably expressed from
14 a single subgenomic RNA to produce structural polyprotein pp2.
15
16
17
18
19
20
21

251 **AAbV Protein Bioinformatics**

252 To annotate the functional protein domains encoded in the AAbV genome, a series
253 of bioinformatics tools were used. Wherever possible, we have followed the
254 convention of *SARS-associated coronavirus* (SARS-CoV) species in naming
255 domains and polyprotein processing products (Ref?). When run against the PDB
256 database, HHPred (Söding et al., 2005) predicts function based on structure. For
257 domains like the polymerase where a nidovirus structure is not yet available, HHPred
258 can sometimes detect a match to a homologous protein, such as the picornavirus
259 polymerase.
30
31
32
33
34
35
36
37
38
39

40 HHPred produced confident predictions for a coronavirus-like M^{pro} (Anand et al.,
41 2002) in pp1a (Fig. 3D). In pp1b HHPred identified a picornavirus-like RNA-
42 dependent RNA polymerase (RdRp (te Velthuis et al., 2009)), nsp13 metal-binding
43 helicase (Deng et al., 2014; Ivanov et al., 2004), nidovirus-specific nsp14
44 exonuclease (ExoN (Ma et al., 2015)) and nsp14 N7 methyltransferase (N7 MTase
45 (Chen et al., 2009; Ma et al., 2015)). In pp2, HHPred identified a chymotrypsin-like
46 serine proteinase (Birktoft and Blow, 1972), a feature analogous to the alphavirus
47 capsid proteinase (Melancont and Garoff, 1987), but until now predicted in only one
48 nidovirus, TurrNV. We have termed this the structural proteinase (S^{pro}).
49
50
51
52
53
54
55
56
57
58

59 Where HHPred was unable to annotate a region, a protein BLAST search was
60 carried out to identify likely homologs among other known nidoviruses. When a
61
62
63
64
65

273 match was found, both proteins were aligned using Clustal Omega (Sievers et al.,
1
274 2011), and the multiple sequence alignment was used in HHpred. The most
3
275 consistent matches to AAbV were from TurrNV. This identified a larger region and a
4
276 more confident match to the coronavirus nsp14 ExoN-N7 MTase.
5
277
6
278 Protein BLAST was used to map the AAbV nidovirus RdRp-associated nucleotidyl
7
279 transferase (NiRAN) and nsp16 2O-MTase domains to homologous domains from
8
280 other nidoviruses. The corresponding regions of AAbV and the top protein BLAST
9
281 match were then submitted to HHpred in align mode, which uses predicted structure
10
282 and primary sequence data to compare proteins. This led to confident identifications
11
283 of the NiRAN and a match for the divergent but functional 2O MTase domain of Gill-
12
284 associated virus (Zeng et al., 2016). One other uncharacterized domain was also
13
285 identified in both AAbV and TurrNV by protein BLAST, in the position where the
14
286 coronavirus conserved replication accessory proteins nsp7-10 were expected (Fig.
15
287 3D). However, there was not enough similarity between the AAbV-TurrNV
16
288 conserved domain and other nidovirus domains to confidently assign a function to
17
289 this region.
18
290
19
291 We also looked for transmembrane regions which are typically clustered in three
20
292 regions in nidovirus pp1a. Domain-level maps of new and known nidoviruses pp1a
21
293 and pp1b are shown in Figs. 4 and 5A, respectively. Nidoviruses typically have a
22
294 cluster of an even number of transmembrane helices near the midpoint of pp1a,
23
295 equivalent to nsp3 of SARS coronavirus. Nidoviruses also have two other clusters of
24
296 2-8 transmembrane helices flanking the M^{pro} domain from both sides.
25
297
26
298 AAbV is also missing some common but not universally conserved nidovirus
27
299 domains. AAbV does not appear to encode a homolog of the uridylate-specific
28
300 nidovirus endonuclease (NendoU), nor is there enough un-annotated protein
29
301 sequence in pp1b to accommodate an NendoU. This result is in line with the lack of
30
302 this domain in other invertebrate nidoviruses (Nga et al., 2011). We were also not
31
303 able to corroborate the prediction (Debat, 2018) of a papain-like proteinase domain
32
304 situated among the predicted transmembrane regions of the first transmembrane
33
305 cluster, or of a potential S-like domain of the structural polyprotein.
34
306
35
36
37
38
39
307
40
310
41
312
42
314
43
316
44
318
45
320
46
322
47
324
48
326
49
328
50
330
51
332
52
334
53
336
54
338
55
340
56
342
57
344
58
346
59
348
60
350
61
352
62
354
63
356
64
358
65

307 The pp2 gene of AAbV encodes a putative structural polyprotein of 3224 amino
1 acids. HHPred and BLAST were not able to detect matches for any domains except
2 S^{pro} in AAbV pp2. TMHMM (Krogh et al., 2001) predicted 13 transmembrane helices
3 in pp2, which were generally arranged in pairs with large intervening domains, which
4 we have tentatively named S^{pro}, predicted surface glycoproteins GP1-3 and a
5 possible nucleoprotein (Fig. 5B). Included in pp2 are additional smaller domains that
6 have not been named yet, pending a better understanding of pp2 proteolytic
7 processing. SignalP (Petersen et al., 2011) predicted an initial signal peptide at the
8 extreme amino terminus, but after removing the predicted signal peptide and re-
9 running the prediction with the “N-terminal truncation of input sequence” parameter
10 set to zero, a total of six potential signal peptidase cleavage sites were detected.
11
12 The identification of the nucleoprotein-like domain is based on a resemblance to the
13 N proteins of *Bovine torovirus* and *Alphamesonivirus 1*, and to the carboxyl-terminal
14 half of the SARS-CoV N. The features the AAbV N-like protein shares with N of
15 other established nidoviruses are an initial glycine-rich region that may be flexibly
16 disordered, followed by a lysine and arginine-rich region from amino acid 2869-2913
17 that could facilitate RNA binding, followed by a domain predicted by PSIPRED
18 (Buchan et al., 2013) to contain a secondary structure profile similar to that of the
19 Equine arteritis virus N and the SARS-CoV N carboxyl-terminal domain. We did not
20 find strong evidence to support the analysis of Debat (Debat, 2018) predicting a
21 spike-like fold in GP3, but we concur with Debat in noticing that GP2 (and we would
22 add, GP3) have a protein secondary structure profile that resembles an alphavirus
23 E1 protein and the E1-like protein of TurrNV.
24
25
26
27
28
29
30
31
32
33
34
35
36
37
38
39
40
41
42
43
44
45
46
47
48
49
50
51
52
53
54
55
56
57

330 One previous report (Prince, 2003) had noted virus-like particles described as
331 resembling intracellular alphavirus virions, that were widespread in transmission
332 electron micrographs of *Aplysia californica* tissue, which would seem to be
333 consistent with the alphavirus-like organization of the structural polyprotein and
334 apparent E1 homology. However, further testing is necessary to confirm whether
335 those virus-like particles are related to AAbV.
336
337

338 **AAbV Proteinases**

339 When identifying viruses through bioinformatics, there is a risk that the sequences
340 are either mis-assembled, contain errors, or are artifacts of the sequencing and
61
62
63
64
65

341 sequence assembly processes. We tested the function of some AAbV protein
1 features to determine if any was biologically functional, as a way to better assess
2 whether the AAbV genome represented a replicating virus encoding functional parts.
3
4
5
6

7 The AAbV M^{pro} and S^{pro} plus surrounding regions up to the nearest preceding and
8 following predicted transmembrane helix were cloned into pTriEx 1.1 and expressed
9 with an amino-terminal herpes simplex virus epitope (HSV) tag, and a carboxyl-
10 terminal poly-histidine (HIS) tag. Expressions were carried out by *in vitro* coupled T7
11 transcription and rabbit reticulocyte lysate translation. M^{pro} cleavage at an amino-
12 terminal site was detected by the presence of an approximately 16 kDa HSV-tagged
13 fragment (Fig. 6), which would be expected if M^{pro} cleavage occurred in the vicinity of
14 amino acid 4375, located near the start of the region of M^{pro} homology at amino acid
15 4401 (Fig. 3D). S^{pro} was expressed, but did not produce any detectable cleavage
16 products in the same assay (data not shown). From this we concluded that AAbV
17 M^{pro} appeared to have proteinase activity in the context of our expression construct,
18 while our S^{pro} construct did not. Further work will be needed to determine whether
19 the failure of the putative S^{pro} to cleave was a result of the construct boundaries,
20 assay conditions, lack of an appropriate substrate, or errors in the protein sequence.
21
22
23
24
25
26
27
28
29
30
31
32
33
34
35
36
37
38
39
40
41
42
43
44
45
46
47
48
49
50
51
52
53
54
55
56
57
58
59
60
61
62
63
64
65

360 To further characterize the activity of AAbV M^{pro}, alanine-scanning mutations were
361 made to amino acids that appeared to match the catalytic cysteine and histidine
362 residues of other coronavirus main proteinases. Mutation of the putative catalytic
363 histidine H4429 did not strongly reduce proteolytic processing, while mutation of the
364 cysteine C4538 blocked proteinase activity (Fig. 6). These data demonstrate that
365 AAbV encodes at least one functional proteinase, but further work is needed to
366 determine the cleavage specificity and map proteolytic processing by the AAbV M^{pro}.
367
368

AAbV pp1ab expression

369 Another unusual feature of AAbV was the presence of an in-frame stop codon
370 separating the pp1a and pp1b genes, rather than the expected ribosomal frameshift
371 signal found in most other nidoviruses. We note that an in-frame stop codon
372 separates the putative pp1a and pp1b of the molluscan nidovirus Tunninivirus 1,
373 which was phylogenetically grouped with AAbV and *Alphamesonivirus 1* (Fig. 1).
374 This suggested that AAbV may use a translational termination-suppression signal as

375 a way to control expression of the pp1b region. Termination-suppression signals are
1 376 found in several other viruses including alphaviruses and some retroviruses, and
2 377 typically consist of a UAG or UGA stop codon followed by an RNA secondary
3 378 structure element, and the efficiency of suppression normally depends on the stop
4 379 codon, the nucleotides immediately following the stop codon, and the free energy of
5 380 the RNA secondary structure element (Feng et al., 1992). The pp1a gene of AAbV
6 381 ends in a UGA stop codon, and the region that follows was predicted by Mfold
7 382 (Zuker, 2003) to be capable of forming several related RNA secondary structure
8 383 elements, of which the most consistently predicted is shown in Fig. 7A. A potential
9 384 pseudoknot-like conformation in the same region is shown by Debat (Debat, 2018).
10
11
12
13
14
15
16
17
18
19
20
21
22
23
24
25
26
27
28
29
30
31
32
33
34
35
36
37
38
39
40
41
42
43
44
45
46
47
48
49
50
51
52
53
54
55
56
57
58
59
60
61
62
63
64
65

385
386 To investigate protein expression at the pp1a-pp1b region, nucleotides 17255 to
387 17707 were cloned into pTriex 1.1 with amino-terminal HSV and carboxyl-terminal
388 HIS tags. This construct would allow detection and quantification of the 25 kDa
389 proteins that stopped at the natural UGA stop codon that would have an HSV tag
390 only, and 35 kDa readthrough products that would have both HSV and HIS tags.
391 Expression of this construct produced the expected 25 kDa termination product and
392 35 kDa readthrough product (Fig. 7B-D). Based on densitometry analysis (not
393 shown), it was estimated that 25-30% of translation events resulted in readthrough.
394

395 The choice of stop codon and elements of the two codons that follow have been
396 shown to affect the efficiency of translational termination (Cridge et al., 2018;
397 Skuzeski et al., 1991). To further investigate the AAbV termination-suppression
398 signal, constructs were made in which the region around the pp1a stop codon was
399 perturbed from the wild-type UGAC, predicted to produce near optimal termination,
400 to UAAA, predicted to produce much less than optimal termination. In another
401 construct, 42 nucleotides predicted to form one side of the predicted RNA stem-
402 loops were deleted (Δ 42; Fig. 7A). Mutation of the AAbV pp1a stop codon had little
403 effect on readthrough efficiency (Fig. 7B), but deletion of 42 nucleotides predicted to
404 be involved in RNA secondary structures appeared to decrease readthrough, and led
405 to a smaller readthrough product as predicted. Together these results indicate that
406 the pp1b region of AAbV is probably expressed by readthrough of a UGA stop

407 codon, mediated by a functional termination-suppression signal that is dependent on
1 sequences following the stop codon.
2
3
4
5

6 MLeV genome

7 Microhyla letovirus is represented by a single assembly (accession number
8 GECV01031551) of 22304 nucleotides that potentially encodes a partial corona-like
9 virus from near the end of a protein equivalent to SARS-CoV nsp3 to the 3'-end (Fig.
10 8A). No other matches for this sequence were found in the TSA or EST databases
11 by nucleotide BLAST. The host organism of MLeV is shown in Fig. 8B. Mapping
12 single sequence reads onto the genome revealed a strong age dependence of MLeV
13 detection. The number of fragments per kilobase of transcript per million mapped
14 reads decreased by seven-fold from pre-metamorphosis to metamorphic climax,
15 then decreased again by fourteen-fold from metamorphic climax to completion of
16 metamorphosis. Further testing was done by reverse transcriptase polymerase
17 chain reaction using MLeV-specific primers on the same population of adult frogs
18 later in the year, but all the adult material tested was negative for MLeV (LZ,
19 personal communication).

20
21
22
23
24
25
26
27
28
29
30
31
32
33
34
35
36
37
38
39
40
41
42
43
44
45
46
47
48
49
50
51
52
53
54
55
56
57
58
59
60
61
62
63
64
65

The MLeV genome is missing the 5'-end of the genome, including a 5'-untranslated region and sequences corresponding to coronavirus nsp1, nsp2 and part of nsp3.

The size of the missing part of the genome can be estimated at 1500-4000 nucleotides based on comparison to complete genomes from the relatively small deltacoronaviruses or the relatively large alphacoronaviruses. The MLeV genome contains a 572 nucleotide 3'-untranslated region and an 18-nucleotide polyadenosine tail.

The genome organization of MLeV was similar to that of coronaviruses, with a predicted -1 ribosomal frameshift signal. Usually, a programmed -1 ribosomal frameshift signal consists of three elements: a slippery sequence that is most commonly UUUAAAC in coronaviruses, a stop codon for the upstream coding region, and a strong RNA secondary structure or pseudoknot. MLeV encodes a potential slippery sequence at nucleotide 6085 (UUUAAAC) followed immediately by a UAA stop codon for pp1a. The region following the putative frameshift signal was predicted by Mfold to adopt a stem-loop conformation which may be part of an RNA

441 pseudoknot (not shown), but further biological characterization is needed to
1 442 determine the boundaries of the frameshifting region and test its frameshifting
2 443 efficiency.
3 444
4 445

5 446 The 3'-end of the MLeV genome contains six ORFs that could encode proteins of 50
6 447 or more amino acids, which presumably include the viral structural proteins. Five of
7 448 the six 3'-end ORFs are preceded by a sequence UCUAAHA (where H is any
8 449 nucleotide except G), that resembles the UCUAAAC transcription regulatory
9 450 sequence of the coronavirus mouse hepatitis virus. These candidate transcription-
10 451 regulatory sequences start 6-66 nucleotides before the AUG start codon of the next
11 452 ORF. Without the 5'-end or any evidence of viral subgenomic RNAs, it is not
12 453 possible to be certain how the 3'-end ORFs are expressed, but these repeated
13 454 sequences are evidence that MLeV may express its structural proteins from
14 455 subgenomic RNAs in the manner of coronaviruses. Unfortunately, the original RNA
15 456 sample that was used for *Microhyla fissipes* transcriptomic analysis was completely
16 457 consumed, and could not be further tested by RT-PCR.
17 458
18 459

19 460 The first of these downstream ORFs encodes a large S-like protein of 1526 amino
20 461 acids with an amino-terminal signal peptide predicted by SignalP and a carboxyl-
21 462 terminal transmembrane region predicted by TMHMM. The second and third ORFs
22 463 appear to encode a unique single-pass transmembrane protein of 55 amino acids
23 464 (ORF 2b) and a unique soluble 157 (ORF 3) amino acid protein, respectively, which
24 465 are likely strain-specific accessory proteins. The fourth ORF encodes an E-like
25 466 protein of 77 amino acids, with an amino-terminal predicted transmembrane region
26 467 followed by a potential amphipathic helix predicted by Amphipaseek (Sapay et al.,
27 468 2006). The fifth ORF encodes a 241 amino acid long three-pass transmembrane
28 469 protein that resembles the coronavirus M protein, and the sixth ORF encodes a
29 470 putative N protein of 459 amino acids. Together, these 3'-ORFs appear to encode a
30 471 complete coronavirus functional repertoire, and are present in the same order found
31 472 on all other currently known coronavirus genomes (Neuman and Buchmeier, 2016).
32 473 The start codons of the putative S and M ORFs appear to overlap with the stop
33 474 codons of preceding ORFs, indicating a relatively compact genome.
34 475
35 476
36 477
37 478
38 479
39 480
40 481
41 482
42 483
43 484
44 485
45 486
46 487
47 488
48 489
49 490
50 491
51 492
52 493
53 494
54 495
55 496
56 497
57 498
58 499
59 500
60 501
61 502
62 503
63 504
64 505
65 506

474 To test whether there was support for MLeV subgenomic RNA species in the raw
1 sequence data, individual sequence reads were mapped to the MLeV genome using
2 the same method used for AAbV above (Fig. 9A). There was not a noticeable
3 change in read depth at the junction between ORFs 1a and 1b of MLeV, suggesting
4 that polyprotein 1b is expressed by a translational rather than transcriptional
5 mechanism. However, there were two sudden increases of about eight-fold in read
6 depth immediately before the start of the N ORF and near the beginning of the
7 adjacent E and M ORFs (Fig. 9B). Expected increases in read depth before the
8 putative S gene and the largest putative accessory gene were not detected. As with
9 AAbV, many low-frequency sequence variants were detected in the raw sequence
10 data, but no indels were consistently present in the region surrounding the putative
11 transcription-regulatory sequences. These data suggest that at least the M and N
12 genes of MLeV are expressed via subgenomic mRNAs.
13
14

15 **MLeV Protein Bioinformatics**

16 In the pp1a region, HHPred detected matches for conserved coronavirus domains
17 including the carboxyl-terminal domain of coronavirus nsp4, M^{pro}, nsp7, nsp8, nsp9
18 and nsp10 (Fig. 8C). In the pp1b region, HHPred detected matches for a
19 picornavirus-like RdRp, the nsp13 metal-binding helicase, the nsp14 ExoN-N7
20 MTase, the nsp15 NEndoU, and the nsp16 2O MTase. In the structural protein
21 region, HHPred detected a match for the amino-terminal domain of coronavirus N in
22 the putative MLeV N protein.
23
24

25 As with AAbV, we then widened our search to include conserved coronavirus
26 domains that do not yet have known protein structures. This led to a match for the
27 carboxyl-terminal region of nsp3, amino-terminal region of nsp4, nsp6, the nsp12
28 NiRAN domain, and a match between coronavirus M and the proposed MLeV M
29 protein. Neither the proposed MLeV S nor E protein could be further corroborated by
30 bioinformatics tools. Together, this indicated that MLeV appears to encode a
31 complete set of conserved coronavirus-like proteins from the carboxyl-terminal
32 region of nsp3 through the end of the genome.
33
34

35 **Discussion and Conclusions**

36
37
38
39
40
41
42
43
44
45
46
47
48
49
50
51
52
53
54
55
56
57
58
59
60
61
62
63
64
65

507 With the addition of MLeV, AAbV and a host of other recently-published highly
1 508 divergent nidoviruses, the field of nidovirus evolution is due for a revision, which will
2 509 require a detailed approach and that will fit best in another study. However, a few
3 510 tentative conclusions can be drawn from these new viruses.
4
5 511
6
7 512 Firstly, the new viruses confirm that the region of pp1a up to the SARS-CoV nsp4
8 513 equivalent, which seems to contain a variety of anti-host countermeasures in the
9 514 viruses where this region has been studied (Neuman et al., 2014), is highly variable
10 515 and does not appear to contain any universally-conserved domains. As previously
11 516 noted (Lauber et al., 2013), this part of the genome appears to have the most
12 517 genetic flexibility, even within viral genera, and likely has great relevance to those
13 518 studying interactions between viruses and innate immunity (Bailey-Elkin et al., 2014;
14 519 Lokugamage et al., 2015; Mielech et al., 2014). It is worth noting that the region
15 520 preceding the M^{pro} in AAbV is over 13 kb – larger than most other complete RNA
16 521 virus genomes.
17
18 522
19
20 523 Secondly, two elements of genome architecture seem to be conserved throughout
21 524 the *Nidovirales*: a M^{pro} flanked by multi-pass transmembrane regions, and the block
22 525 containing NiRAN-RNA polymerase-metal binding-Helicase. Knowledge of these
23 526 apparent nidovirus genetic synapomorphies should make it possible to design
24 527 searches to detect even more divergent nido-like viruses in transcriptomes.
25
26
27 528
28
29
30 529 Thirdly, the NendoU domain appears to be found only in viruses infecting vertebrate
31 530 animals, and is lacking in every known nidovirus-like genome from an invertebrate
32 531 host. This suggests that the function of NendoU may have evolved as a
33 532 countermeasure to conserved metazoan viral RNA recognition machinery involved in
34 533 innate immunity (Lokugamage et al., 2015).
35
36
37 534
38
39
40 535 Fourthly, while most currently known nidovirus species are associated with terrestrial
41 536 hosts, the greatest phylogenetic diversity of nidoviruses is now associated with hosts
42 537 that live in aquatic environments. Since terrestrial metazoan transcriptomes are
43 538 relatively well-sampled in comparison to aquatic and particularly marine metazoa, we
44 539 would predict this trend is likely to continue. Of the eight proposed nidovirus
45 540 families shown in Figs. 4 and 5, four contain only viruses associated with aquatic
46
47
48
49
50
51
52
53
54
55
56
57
58
59
60
61
62
63
64
65

541 hosts, two (*Arteriviridae* (Shi et al., 2018) and the proposed *Tobaniviridae*) are found
542 in a mix of strictly aquatic and strictly terrestrial animals, and two (*Coronaviridae*,
543 *Mesoniviridae*) are in part associated with hosts such as mosquitoes and frogs that
544 have an obligate aquatic larval phase. Taken together, this data suggests that it may
545 be useful to consider potential routes of interspecies transmission between marine,
546 freshwater and terrestrial hosts in future studies of nidovirus evolution, as more data
547 becomes available.

548
549 Lastly, the structural protein repertoire of nidoviruses appears to be quite broad
550 compared to other known virus orders. There do not appear to be any conserved
551 nidovirus structural proteins with the possible exception of the nucleoprotein
552 (discussed elsewhere (Neuman and Buchmeier, 2016)), and even that homology can
553 only be regarded as hypothetical until more structures of putative nucleoproteins are
554 solved. A tentative categorization of nidovirus structural proteins, based on size,
555 predicted transmembrane regions, and predicted protein secondary structure is
556 shown in Fig. 10. If correct, this would indicate that nidoviruses have a diverse set of
557 structural proteins that includes a variety of possibly unrelated spike-like proteins
558 plus components shared with *Orthomyxoviridae* (HA and HE), *Togaviridae* (E1 and
559 the E3 structural serine proteinase), *Flaviviridae* (the capsid RNase). This structural
560 repertoire appears to be variously expressed from subgenomic RNAs encoding a
561 single gene (as proposed for MLeV), giant polyproteins such as that of AAbV, and a
562 mix of intermediate-sized polyproteins and single genes, as in the *Roniviridae*.
563 Taken together, these observations suggest that structural proteins are widely
564 shared and exchanged among RNA viruses, and that conserved elements of the
565 replicase will be more useful than structural proteins for anyone trying to construct
566 trees that connect viruses at taxonomic ranks above the family level.

567
568 **Materials and methods**

569
570 **Phylogeny**

571 Nidovirus phylogeny was reconstructed based on MSA of concatenated M^{pro} ,
572 NiRAN, RdRp, CH cluster and SF1 Helicase conserved cores (3417-3905, 5441-
573 5866, 6095-7291, 7340-7504, 7781-8545 nt of the Equine arteritis virus genome
574 X53459.3), prepared with the help of Viralis platform (Gorbalenya et al., 2010).

575 Representatives of 28 nidovirus species (Supplementary table 1) delineated in
1
576 recent ICTV proposals (Brinton et al., 2017; Gorbalenya et al., 2017b, 2017a;
2
577 Ziebuhr et al., 2017) were used. Phylogeny was reconstructed by IQ Tree 1.5.5
3
578 using a partition model where the evolutionary model for each of the five domains
4
579 was selected by ModelFinder (Chernomor et al., 2016; Kalyaanamoorthy et al.,
5
580 2017; Nguyen et al., 2015). To estimate branch support, Shimodaira-Hasegawa-like
6
581 approximate likelihood ratio test (SH-aLRT) with 1000 replicates was conducted.
7
582 The tree was midpoint rooted and visualised with the help of R packages APE 3.5
8
583 and phangorn 2.0.4(Paradis et al., 2004; R Development Core Team, 2011; Schliep,
9
584 2011).
10
585
11
586 **Protein assays**
12
587 Nucleotides 12926-14176 containing the AAbV M^{pro} and flanking regions extending
13
588 to the preceding and following predicted transmembrane regions was produced as a
14
589 synthetic GeneArt Strings DNA fragment (Invitrogen). This was used as the template
15
590 in a 50 µl PCR reaction using primers Aby_IF_MP_F
16
591 (CCCGAGGATCTCGAGTTGCGAATGATTTGTCTACC) and Aby_IF_MP_R
17
592 (GATGGTGGTGCTCGAGACACAGACAACACAACAAAAAA) with 1x Phusion High
18
593 Fidelity PCR Mastermix (Thermo Fisher Scientific). The 1283 bp PCR product was
19
594 gel extracted using a QIAquick gel extraction kit (Qiagen) and cloned into pTriEx1.1
20
595 (Novagen / Merck) linearised with *Xhol* using In-Fusion HD cloning reagents
21
596 (Clontech). 2 µl of the In-Fusion reaction was transformed into Stellar chemically
22
597 competent cells as per the manufacturers protocol (Clontech) and selected on LB
23
598 agar containing 100 ug/mL ampicillin. The final construct with a T7 RNA polymerase
24
599 promoter and in-frame amino-terminal HSV and carboxyl-terminal HIS tags was
25
600 verified by Sanger sequencing (Source Bioscience) of plasmid DNA purified using a
26
601 QIAquick spin miniprep kit (Qiagen). Site-directed mutagenesis was carried out using
27
602 the Quikchange II (Agilent) reagents and protocol. Protein expression was carried
28
603 out in a 50 µl reaction volume using 0.5 µg of plasmid DNA with the TnT® Quick
29
604 Coupled Transcription/Translation System (Promega) reagents and protocol. In vitro
30
605 transcription and translation was carried out for 1h.
31
606
32
607 Samples containing expressed proteins were mixed with an equal volume of 2× SDS
33
608 PAGE loading buffer containing 100mM Tris-HCL pH6.8, 4% w/v SDS, 20% w/v
34
609
35
610
36
611
37
612
38
613
39
614
40
615
41
616
42
617
43
618
44
619
45
620
46
621
47
622
48
623
49
624
50
625
51
626
52
627
53
628
54
629
55
630
56
631
57
632
58
633
59
634
60
635
61
636
62
637
63
638
64
639
65

609 glycerol, 0.2% bromophenol blue, 2% β - mercaptoethanol. Samples were boiled at
1 610 100°C for 10 minutes, collected by gentle centrifugation, and loaded in Mini-
2 611 PROTEAN precast polyacrylamide gels (BioRad). After electrophoresis, proteins
3 612 were blotted to PVDF membranes for 80 mins at 150mA using a Trans-Blot Turbo
4 613 (BioRad). Membranes were blocked overnight at 4°C with 5% (w/v) non-fat milk
5 614 powder in TBST (50 mM Tris, 150 mM NaCl, 0.1% Tween 20, pH 7.5). Membranes
6 615 were then washed three times for 5 min each on a rocking platform at 25 rpm with
7 616 TBST buffer before addition unconjugated rabbit anti-HIS tag monoclonal antibody
8 617 (Abcam) or unconjugated rabbit anti-HSV tag monoclonal antibody (Abcam) for 1
9 618 hour. Membranes were again washed three times for 5 min each with TBST buffer
10 619 before addition of horseradish peroxidase-conjugated goat anti-rabbit secondary
11 620 antibody for 1 hour. For detection, ChemiFast chemiluminescent reagent (Syngene)
12 621 was used to detect bound secondary antibody. Samples were visualized using a
13 622 Syngene Chemi XL G:Box gel documentation system. Gel images were cropped
14 623 and brightness and contrast of images was adjusted using GIMP software (GIMP
15 624 team).
16 625
17 626

31 626 The region from the pp1a-pp1b junction containing the putative termination-
32 627 suppression signal of AAbV, nucleotides 17255-17707, was PCR amplified from a
33 628 synthetic GeneArt Strings fragment (Invitrogen) using primers Aby_IF_SS_F
34 629 (CCCGAGGATCTCGAGGAGTCTTGTGCGTGAAGT) and Aby_IF_SS_R
35 630 (GATGGTGGTGCTCGAGAGGATTAATCCGTCTGTCAA). The predicted S^{pro}-
36 631 containing region of AAbV, nucleotides 25918-27183, was PCR amplified from a
37 632 synthetic GeneArt Strings fragment (Invitrogen) using primers Aby_IF_TryP_R
38 633 (GATGGTGGTGCTCGAGCGGTTGTTCGCATACAGA) and Aby_IF_TryP_R
39 634 (GATGGTGGTGCTCGAGCGGTTGTTCGCATACAGA). Both the S^{pro} and putative
40 635 pp1a-pp1b termination-suppression signal products were cloned, expressed and
41 636 detected in the same way as AAbV M^{pro}.
42 637
43 638

***Microhyla* prevalence**

54 639 Data for the MLeV prevalence study comes from a published report (Zhao et al.,
55 640 2016). Briefly, nine tadpoles were sacrificed, using three individuals from each of the
56 641 three developmental stages as independent biological replicates. One microgram of
57
58
59
60
61
62
63
64
65

642 mRNA of each stage sample was sequenced on an Illumina HiSeq 2000 platform by
1 643 NovoGene (Beijing), and paired-end reads were generated.
2
3
4
5

644 645 **Acknowledgements** 6

7 646 A.A.G. is a PhD student with Alexander E. Gorbaleyna (A.E.G.) and her work and
8 resources she used were partially supported by EU Horizon2020 EVAg 653316 grant
9 and LUMC MoBiLe program to A.E.G. She thanks Igor A. Sidorov, Dmitry V.
10 648 Samborskiy, and A.E.G. for help with the dataset used in her analysis. The work of
11 649 L.Z., G.S. and J.J. was supported by a key project from Chinese Academy of
12 650 Sciences (KJZD-EW-L13) and the National Natural Science Foundation of China
13 651 (No. 31471964). K.B. was supported by a studentship from the Ministry of Education
14 652 in Saudi Arabia (S13280). K.B. thanks Ian M. Jones of the University of Reading for
15 653 assistance in planning and carrying out protein expression and detection studies.
16 654
17 655
18

25 656 **Figure Legends** 26

27 657 **Figure 1. Nidovirus phylogeny reconstructed based on concatenated MSA of**
28 **five replicative domains universally conserved in nidoviruses.** SH-aLRT branch
29 support values are depicted by shaded circles. Species names that are not currently
30 recognized by ICTV are written in plain font. Asterisks designate viruses described in
31 659 this study.
32 660
33 661
34 662
35 663

36 664 **Figure 2. Sequence coverage of AAbV in public NCBI libraries.** (A) Examples of
37 the host organism *Aplysia californica* at swimming veliger, settled, metamorphic,
38 665 juvenile and adult developmental stages (images not to scale, adapted from
39 (Heyland et al., 2011; Moroz et al., 2006)). Summary of distinct sequence
40 666 assemblies and reads in the TSA (B) and EST (C) matching AAbV for which the
41 667 nucleotide BLAST E value was 2×10^{-70} or smaller. (D) Map of AAbV, showing the
42 668 location of the replicase polyprotein genes (ORF1a, ORF1b), structural polyprotein
43 669 gene (ORF2) and poly-adenosine tail (A_n). The position of sequences from the TSA
44 670 (E) and EST (F) databases matching AAbV is shown.
45 671
46 672
47 673

48 674 **Figure 3. Coding capacity, depth of coverage and bioinformatics of AAbV.** (A)
49 675 Genome and coding capacity of AAbV and SARS-CoV are shown to scale. (B) Total
50 676 depth of coverage based on a sample of 672017 aligned spots matching AAbV from
51 677
52 678
53 679
54 680
55 681
56 682
57 683
58 684
59 685
60 686
61 687
62 688
63 689
64 690
65 691

676 *Aplysia californica* RNA sequence read archives including SRR385787, SRR385788,
1 677 SRR385792, SRR385793, SRR385795, SRR385800, SRR385802 and SRR385815.
2 678 The putative start site of a viral subgenomic RNA species is marked with an arrow.
3 679 (C) Alignment of the 5'-untranslated region and the intergenic sequence between the
4 680 pp1b and pp2 genes showing a potential transcription-regulatory sequence (boxed).
5 681 (D) Bioinformatic assignment of domains in AAbV. Sequence(s) used for prediction
6 682 (Input) were either AAbV alone or a multiple sequence alignment containing AAbV
7 683 and TurrNV. Probability score from HHpred and E value from HHpred or BLAST
8 684 are shown. Accession numbers are given for sequences or protein structures
9 685 identified as a match for an AAbV domain (Model).
10 686
11 687
12 688
13 689
14 690
15 691
16 692
17 693
18 694
19 695
20 696
21 697
22 698
23 699
24 700
25 701
26 702
27 703
28 704
29 705
30 706
31 707
32 708
33 709
34 710
35 711
36 712
37 713
38 714
39 715
40 716
41 717
42 718
43 719
44 720
45 721
46 722
47 723
48 724
49 725
50 726
51 727
52 728
53 729
54 730
55 731
56 732
57 733
58 734
59 735
60 736
61 737
62 738
63 739
64 740
65 741

Figure 4. Comparison of predicted domain-level organization in polyprotein 1a of new viruses to previously described nidoviruses. Gaps have been introduced so to align predicted homologous domains. Virus naming and taxonomy conventions follow the ICTV proposals in which MLeV and AAbV were first described (Gorbalenya et al., 2017b, 2017a; Ziebuhr et al., 2017). New viruses are marked with stars, accepted taxonomic ranks are italicized and proposed taxonomic ranks are not italicized. Polyprotein processing products from SARS-CoV are shown at top. Domains are colored to indicate predicted similarity to SARS-CoV nsp1 (CoV nsp1), SARS-CoV nsp2 (nsp2-like), ubiquitin (Ub-like), macrodomains, papain-like proteinase (PL^{pro}), first section of the coronavirus Y domain (CoV Y1), first section of the arterivirus Y domain (ArV Y1) coronavirus-specific Y domain-like (CoV Y-like), carboxyl-terminal domain of coronavirus nsp4 (nsp4 CTD-like), region with PSIPRED predicted structural similarity to nsp4 CTD, main proteinase (M^{pro}), SARS-CoV nsp8-like (CoV nsp8), Equine arteritis virus nsp7 α (ArV nsp7 α), SARS-CoV nsp10 (CoV nsp10), protein kinase-like (Kinase), RNA methyltransferase (Mtase), potential metal ion-binding clusters with 4 cysteine or histidine residues in a 20 amino acid window (CH-cluster), transmembrane helices, hydrophobic transmembrane-like regions that may not span the membrane by analogy to coronavirus nsp4 and nsp6 (TM-like) and disordered regions (Unstructured).

Figure 5. Comparison of predicted domain-level organization in polyprotein 1b of new viruses to previously described nidoviruses. (A) Domains include the nidovirus RdRp-associated nucleotidyl transferase (NiRAN), RdRp, potential metal

710 ion binding clusters with four cysteine or histidine residues in a window of 20 amino
1 acids (CH cluster), homologs of the domain of unknown function in the middle of
2 coronavirus nsp13 (CoV nsp13b), superfamily 1 helicase (SF1 Helicase), nidovirus-
3 specific exonuclease (ExoN) and uridylate-specific endonuclease (NEndoU), RNA
4 cap N7 methyltransferase (N7 MTase) and RNA cap 2'-O-methyltransferase (2O
5 MTase). (B) Domains of pp2 include the structural protease (S^{pro}), putative
6 glycoproteins GP1, GP2 and GP3, and a nucleoprotein-like domain (N?), TMHMM-
7 predicted transmembrane domains and SignalP-predicted signal peptidase cleavage
8 sites.
9
10
11
12
13
14
15
16
17

18 **Figure 6. Investigation of proteinase activity of AAbV M^{pro} .** The AAbV main
19 proteinase (M^{pro} ; A-B) and surrounding regions were expressed as HSV and HIS-
20 tagged constructs as shown in panel A. A white triangle marks the expected size of
21 the 52.5 kDa uncleaved M^{pro} constructs. Black triangles mark the size of
22 approximately 16 kDa amino-terminal cleavage products. Non-specific bands that
23 were also present in control lanes are indicated with a star.
24
25
26
27
28
29
30

31 **Figure 7. Mutational analysis of the termination-suppression signal (TSS) at**
32 **the ORF1a/b junction.** (A) Schematic view of the TSS expression construct and
33 introduced HSV and HIS tags, showing only predicted RNA secondary structures
34 that were consistent in the best six models generated by Mfold. Mutations around
35 the stop codon (bold, producing the UAAA construct) or removing one side of the
36 predicted stem-loops ($\Delta 42$) are shown. (B-D) Western blots showing translation of
37 mutant TSS expression constructs in a coupled T7 polymerase rabbit reticulocyte
38 lysate expression system. Blots were probed with anti-HSV (B, D) to detect both 25
39 kDa terminated and 32-35 kDa readthrough products, or with anti-HIS (C) to detect
40 only readthrough products.
41
42
43
44
45
46
47
48
49
50

51 **Figure 8. Coding capacity and prevalence of MLeV** (A) Schematic representation
52 of the coding capacity of MLeV compared to SARS-CoV, showing the similarities in
53 genome organization. (B) Prevalence of MLeV transcripts in *Microhyla fissipes* by
54 age, by total number of reads and fragments per kilobase of transcript per million
55 mapped reads (FPKM).
56
57
58
59
60
61
62
63
64
65

744 **Figure 9. Depth of coverage and bioinformatics of MLeV.** (A) Total depth of
1 coverage is based on 275503 aligned spots matching MLeV from *Microhyla fissipes*
2 RNA sequence read archives SRR2418812, SRR2418623 and SRR2418554. The
3 putative start sites of a viral subgenomic RNA species are marked with an arrow.
4 Potential subgenomic RNA start sites not marked by a sharp rise in read depth are
5 indicated with question marks. (B) Positions and usage of putative transcription-
6 regulatory sequences. Termination codons from the preceding gene are underlined,
7 initiation codons of the following gene are in bold. (C) Bioinformatic assignment of
8 domains in MLeV.
9
10
11
12
13
14
15
16
17
18
19
20
21
22
23
24
25
26
27
28
29
30
31
32
33
34
35
36
37
38
39
40
41
42
43
44
45
46
47
48
49
50
51
52
53
54
55
56
57
58
59
60
61
62
63
64
65

753
754 **Figure 10. Speculative annotation of nidovirus structural proteins.** Where
755 structures or functions were not known, proteins were categorized according to
756 general PSIPRED secondary structure profile. Marked domains include coronavirus
757 spike protein homologs (Spike) and structurally similar regions (β - α), alphavirus E1
758 homologs (E1) and structurally similar regions (β α β), coronavirus envelope-like
759 proteins (E-like), coronavirus membrane proteins (M-like) and structurally similar
760 proteins (β), potential nucleoprotein (N-like), chymotrypsin-like structural proteinase
761 (S^{pro}), similar to the bovine viral diarrhea virus structural RNase (BVDV RNase),
762 proteins related to influenza A virus hemagglutinin (HA) or torovirus hemagglutinin-
763 esterase (HE), other viral surface glycoproteins (GP-like), domains of no known
764 function (Unknown), SignalP-predicted signal peptidase cleavage sites (SP
765 cleavage), and potential sites cleaved by unknown proteinases by analogy to other
766 nidovirus structural proteins.
767
768 **References**
769 Altschul, S.F., Gish, W., Miller, W., Myers, E.W., Lipman, D.J., 1990. Basic local
770 alignment search tool. *J. Mol. Biol.* 215, 403–10. [https://doi.org/10.1016/S0022-2836\(05\)80360-2](https://doi.org/10.1016/S0022-2836(05)80360-2)
771
772 Anand, K., Palm, G.J., Mesters, J.R., Siddell, S.G., Ziebuhr, J., Hilgenfeld, R., 2002.
773 Structure of coronavirus main proteinase reveals combination of a chymotrypsin
774 fold with an extra α -helical domain. *EMBO J.* 21, 3213–3224.
775 <https://doi.org/10.1093/emboj/cdf327>
776 Bailey-Elkin, B.A., Knaap, R.C.M., Johnson, G.G., Dalebout, T.J., Ninaber, D.K., Van
777 Kasteren, P.B., Bredenbeek, P.J., Snijder, E.J., Kikkert, M., Mark, B.L., 2014.

778 Crystal structure of the middle east respiratory syndrome coronavirus (MERS-
1 CoV) papain-like protease bound to ubiquitin facilitates targeted disruption of
2 deubiquitinating activity to demonstrate its role in innate immune suppression. *J.*
3 *Biol. Chem.* 289, 34667–34682. <https://doi.org/10.1074/jbc.M114.609644>
4
5 Birktoft, J.J., Blow, D.M., 1972. Structure of crystalline α -chymotrypsin. V. The
6 atomic structure of tosyl- α -chymotrypsin at 2 Å resolution. *J. Mol. Biol.* 68, 187–
7 240. [https://doi.org/10.1016/0022-2836\(72\)90210-0](https://doi.org/10.1016/0022-2836(72)90210-0)
8
9 Brinton, M.A., Gulyaeva, A., Balasuriya, U.B.R., Dunowska, M., Faaberg, K.S.,
10 Goldberg, T., Leung, F.-C., Nauwynck, H.J., Snijder, E.J., Stadejek, T.,
11 Gorbatenya, A.E., 2017. ICTV Pending proposal 2017.012S Expansion of the
12 rank structure of the family Arteriviridae and renaming its taxa.
13
14 Buchan, D.W.A., Minneci, F., Nugent, T.C.O., Bryson, K., Jones, D.T., 2013.
15 Scalable web services for the PSIPRED Protein Analysis Workbench. *Nucleic*
16 *Acids Res.* 41. <https://doi.org/10.1093/nar/gkt381>
17
18 Chen, Y., Cai, H., Pan, J., Xiang, N., Tien, P., Ahola, T., Guo, D., 2009. Functional
19 screen reveals SARS coronavirus nonstructural protein nsp14 as a novel cap
20 N7 methyltransferase. *Proc. Natl. Acad. Sci.* 106, 3484–3489.
21
22 <https://doi.org/10.1073/pnas.0808790106>
23
24 Chernomor, O., Von Haeseler, A., Minh, B.Q., 2016. Terrace Aware Data Structure
25 for Phylogenomic Inference from Supermatrices. *Syst. Biol.* 65, 997–1008.
26
27 <https://doi.org/10.1093/sysbio/syw037>
28
29 Cridge, A.G., Crowe-Mcauliffe, C., Mathew, S.F., Tate, W.P., 2018. Eukaryotic
30 translational termination efficiency is influenced by the 3' nucleotides within the
31 ribosomal mRNA channel. *Nucleic Acids Res.* 46, 1927–1944.
32
33 <https://doi.org/10.1093/nar/gkx1315>
34
35 Debat, H.J., 2018. Expanding the size limit of RNA viruses: Evidence of a novel
36 divergent nidovirus in California sea hare, with a ~35.9 kb virus genome.
37
38 bioRxiv.
39
40 Deng, Z., Lehmann, K.C., Li, X., Feng, C., Wang, G., Zhang, Q., Qi, X., Yu, L.,
41 Zhang, X., Feng, W., Wu, W., Gong, P., Tao, Y., Posthuma, C.C., Snijder, E.J.,
42 Gorbatenya, A.E., Chen, Z., 2014. Structural basis for the regulatory function of
43 a complex zinc-binding domain in a replicative arterivirus helicase resembling a
44 nonsense-mediated mRNA decay helicase. *Nucleic Acids Res.* 42, 3464–3477.
45
46 <https://doi.org/10.1093/nar/gkt1310>
47
48
49
50
51
52
53
54
55
56
57
58
59
60
61
62
63
64
65

812 Feng, Y.X., Yuan, H., Rein, A., Levin, J.G., 1992. Bipartite signal for read-through
813 suppression in murine leukemia virus mRNA: an eight-nucleotide purine-rich
814 sequence immediately downstream of the gag termination codon followed by an
815 RNA pseudoknot. *J. Virol.* 66, 5127–5132.

816 Fiedler, T.J., Hudger, A., McKay, S.J., Shivkumar, S., Capo, T.R., Schmale, M.C.,
817 Walsh, P.J., 2010. The transcriptome of the early life history stages of the
818 California Sea Hare *Aplysia californica*. *Comp. Biochem. Physiol. Part D.*
819 *Genomics Proteomics* 5, 165–70. <https://doi.org/10.1016/j.cbd.2010.03.003>

820 Furuya, T., Macnaughton, T.B., La Monica, N., Lai, M.M.C., 1993. Natural evolution
821 of coronavirus defective-interfering rna involves rna recombination. *Virology*
822 194, 408–413. <https://doi.org/10.1006/viro.1993.1277>

823 Gorbalyena, A.E., Brinton, M.A., Cowley, J., de Groot, R., Gulyaeva, A., Lauber, C.,
824 Neuman, B.W., Ziebuhr, J., 2017a. ICTV Pending Proposal 2017.015S.
825 Reorganization and expansion of the order Nidovirales at the family and sub-
826 order ranks.

827 Gorbalyena, A.E., Brinton, M.A., Cowley, J., de Groot, R., Gulyaeva, A., Lauber, C.,
828 Neuman, B.W., Ziebuhr, J., 2017b. ICTV Pending Proposal 2017.014S.
829 Establishing taxa at the ranks of subfamily, genus, sub-genus and species in six
830 families of invertebrate nidoviruses.

831 Gorbalyena, A.E., Lieutaud, P., Harris, M.R., Coutard, B., Canard, B., Kleywelt,
832 G.J., Kravchenko, A.A., Samborskiy, D. V., Sidorov, I.A., Leontovich, A.M.,
833 Jones, T.A., 2010. Practical application of bioinformatics by the multidisciplinary
834 VIZIER consortium. *Antiviral Res.* <https://doi.org/10.1016/j.antiviral.2010.02.005>

835 Heyland, A., Vue, Z., Voolstra, C.R., Medina, M., Moroz, L.L., 2011. Developmental
836 transcriptome of *Aplysia californica*. *J. Exp. Zool. Part B Mol. Dev. Evol.* 316 B,
837 113–134. <https://doi.org/10.1002/jez.b.21383>

838 Ivanov, K.A., Thiel, V., Dobbe, J.C., van der Meer, Y., Snijder, E.J., Ziebuhr, J.,
839 2004. Multiple enzymatic activities associated with severe acute respiratory
840 syndrome coronavirus helicase. *J. Virol.* 78, 5619–32.
841 <https://doi.org/10.1128/JVI.78.11.5619-5632.2004>

842 Kalyaanamoorthy, S., Minh, B.Q., Wong, T.K.F., Von Haeseler, A., Jermiin, L.S.,
843 2017. ModelFinder: Fast model selection for accurate phylogenetic estimates.
844 *Nat. Methods* 14, 587–589. <https://doi.org/10.1038/nmeth.4285>

845 King, A.M.Q., Adams, M.J., Carstens, E.B., Lefkowitz, E.J., 2012. Togaviridae, in:

Virus Taxonomy. pp. 1103–1110.

Krogh, A., Larsson, B., Von Heijne, G., Sonnhammer, E.L.L., 2001. Predicting transmembrane protein topology with a hidden Markov model: Application to complete genomes. *J. Mol. Biol.* 305, 567–580.
<https://doi.org/10.1006/jmbi.2000.4315>

Langmead, B., Salzberg, S.L., 2012. Fast gapped-read alignment with Bowtie 2. *Nat. Methods* 9, 357–359. <https://doi.org/10.1038/nmeth.1923>

Lauber, C., Goeman, J.J., de Parquet, M.C., Thi Nga, P., Snijder, E.J., Morita, K., Gorbatenya, A.E., 2013. The Footprint of Genome Architecture in the Largest Genome Expansion in RNA Viruses. *PLoS Pathog.* 9.
<https://doi.org/10.1371/journal.ppat.1003500>

Lauck, M., Alkhovsky, S. V., Bào, Y., Bailey, A.L., Shevtsova, Z. V., Shchetinin, A.M., Vishnevskaya, T. V., Lackemeyer, M.G., Postnikova, E., Mazur, S., Wada, J., Radoshitzky, S.R., Friedrich, T.C., Lapin, B. a, Deriabin, P.G., Jahrling, P.B., Goldberg, T.L., O'Connor, D.H., Kuhn, J.H., 2015. Historical outbreaks of simian hemorrhagic fever in captive macaques were caused by distinct arteriviruses. *J. Virol.* 89, 8082–7. <https://doi.org/10.1128/JVI.01046-15>

Li, H., Handsaker, B., Wysoker, A., Fennell, T., Ruan, J., Homer, N., Marth, G., Abecasis, G., Durbin, R., Data, G.P., Sam, T., Subgroup, 1000 Genome Project Data Processing, 2009. The Sequence Alignment / Map format and SAMtools. *Bioinformatics* 25, 2078–2079. <https://doi.org/10.1093/bioinformatics/btp352>

Lokugamage, K.G., Narayanan, K., Nakagawa, K., Terasaki, K., Ramirez, S.I., Tseng, C.-T.K., Makino, S., 2015. Middle East Respiratory Syndrome Coronavirus nsp1 Inhibits Host Gene Expression by Selectively Targeting mRNAs Transcribed in the Nucleus while Sparing mRNAs of Cytoplasmic Origin. *J. Virol.* 89, 10970–81. <https://doi.org/10.1128/JVI.01352-15>

Ma, Y., Wu, L., Shaw, N., Gao, Y., Wang, J., Sun, Y., Lou, Z., Yan, L., Zhang, R., Rao, Z., 2015. Structural basis and functional analysis of the SARS coronavirus nsp14-nsp10 complex. *Proc. Natl. Acad. Sci. U. S. A.* 112, 9436–41.
<https://doi.org/10.1073/pnas.1508686112>

Melancont, P., Garoff, H., 1987. Processing of the Semliki Forest virus structural polyprotein: role of the capsid protease. *J. Virol.* 61, 1301–1309.

Mielech, A.M., Chen, Y., Mesecar, A.D., Baker, S.C., 2014. Nidovirus papain-like proteases: Multifunctional enzymes with protease, deubiquitinating and

880 deISGylating activities. *Virus Res.* 194, 184–190.
1 881 <https://doi.org/10.1016/j.virusres.2014.01.025>
2 882 Miranda, J.A., Culley, A.I., Schvarcz, C.R., Steward, G.F., 2016. RNA viruses as
3 883 major contributors to Antarctic vioplankton. *Environ. Microbiol.*
4 884 <https://doi.org/10.1111/1462-2920.13291>
5 885 Moroz, L.L., Edwards, J.R., Puthanveettil, S. V., Kohn, A.B., Ha, T., Heyland, A.,
6 886 Knudsen, B., Sahni, A., Yu, F., Liu, L., Jezzini, S., Lovell, P., Iannucculli, W.,
7 887 Chen, M., Nguyen, T., Sheng, H., Shaw, R., Kalachikov, S., Panchin, Y. V.,
8 888 Farmerie, W., Russo, J.J., Ju, J., Kandel, E.R., 2006. Neuronal Transcriptome of
9 889 Aplysia: Neuronal Compartments and Circuitry. *Cell* 127, 1453–1467.
10 890 <https://doi.org/10.1016/j.cell.2006.09.052>
11 891 Neuman, B.W., Buchmeier, M.J., 2016. Supramolecular Architecture of the
12 892 Coronavirus Particle, in: *Advances in Virus Research*. pp. 1–27.
13 893 <https://doi.org/10.1016/bs.aivir.2016.08.005>
14 894 Neuman, B.W., Chamberlain, P., Bowden, F., Joseph, J., 2014. Atlas of coronavirus
15 895 replicase structure. *Virus Res.* 194, 49–66.
16 896 <https://doi.org/10.1016/j.virusres.2013.12.004>
17 897 Nguyen, L.T., Schmidt, H.A., Von Haeseler, A., Minh, B.Q., 2015. IQ-TREE: A fast
18 898 and effective stochastic algorithm for estimating maximum-likelihood
19 899 phylogenies. *Mol. Biol. Evol.* 32, 268–274.
20 900 <https://doi.org/10.1093/molbev/msu300>
21 901 O'Dea, M.A., Jackson, B., Jackson, C., Xavier, P., Warren, K., 2016. Discovery and
22 902 partial genomic characterisation of a novel nidovirus associated with respiratory
23 903 disease in wild shingleback lizards (*Tiliqua rugosa*). *PLoS One* 11.
24 904 <https://doi.org/10.1371/journal.pone.0165209>
25 905 Paradis, E., Claude, J., Strimmer, K., 2004. APE: Analyses of phylogenetics and
26 906 evolution in R language. *Bioinformatics* 20, 289–290.
27 907 <https://doi.org/10.1093/bioinformatics/btg412>
28 908 Petersen, T.N., Brunak, S., Von Heijne, G., Nielsen, H., 2011. SignalP 4.0:
29 909 Discriminating signal peptides from transmembrane regions. *Nat. Methods*.
30 910 <https://doi.org/10.1038/nmeth.1701>
31 911 Prince, J.S., 2003. A presumptive alphavirus in the gastropod mollusc, *Aplysia*
32 912 *californica*. *Bull. Mar. Sci.* 73, 673–677.
33 913 R Development Core Team, R., 2011. R: A Language and Environment for Statistical
34 914
35 915
36 916
37 917
38 918
39 919
40 920
41 921
42 922
43 923
44 924
45 925
46 926
47 927
48 928
49 929
50 930
51 931
52 932
53 933
54 934
55 935
56 936
57 937
58 938
59 939
60 940
61 941
62 942
63 943
64 944
65 945

914 Computing, R Foundation for Statistical Computing. <https://doi.org/10.1007/978->
1 915 3-540-74686-7
2
3 916 Saberi, A., Gulyaeva, A.A., Brubacher, J., Newmark, P.A., Gorbatenya, A., 2018. A
4 917 planarian nidovirus expands the limits of RNA genome size. *bioRxiv*.
5
6 918 Sapay, N., Guermeur, Y., Deléage, G., 2006. Prediction of amphipathic in-plane
7 919 membrane anchors in monotopic proteins using a SVM classifier. *BMC*
8
9 920 *Bioinformatics* 7. <https://doi.org/10.1186/1471-2105-7-255>
10
11 921 Schliep, K.P., 2011. *phangorn*: Phylogenetic analysis in R. *Bioinformatics* 27, 592–
12 922 593. <https://doi.org/10.1093/bioinformatics/btq706>
13
14 923 Shi, M., Lin, X.D., Chen, X., Tian, J.H., Chen, L.J., Li, K., Wang, W., Eden, J.S.,
15
16 924 Shen, J.J., Liu, L., Holmes, E.C., Zhang, Y.Z., 2018. The evolutionary history of
17
18 925 vertebrate RNA viruses. *Nature* 556, 197–202. <https://doi.org/10.1038/s41586-018-0012-7>
19
20 926
21
22 927 Shi, M., Lin, X.D., Tian, J.H., Chen, L.J., Chen, X., Li, C.X., Qin, X.C., Li, J., Cao,
23
24 928 J.P., Eden, J.S., Buchmann, J., Wang, W., Xu, J., Holmes, E.C., Zhang, Y.Z.,
25
26 929 2016. Redefining the invertebrate RNA virosphere. *Nature* 540, 539–543.
27
28 930 <https://doi.org/10.1038/nature20167>
29
30
31 931 Sievers, F., Wilm, A., Dineen, D., Gibson, T.J., Karplus, K., Li, W., Lopez, R.,
32
33 932 McWilliam, H., Remmert, M., Söding, J., Thompson, J.D., Higgins, D.G., 2011.
34
35 933 Fast, scalable generation of high-quality protein multiple sequence alignments
36
37 934 using Clustal Omega. *Mol. Syst. Biol.* 7. <https://doi.org/10.1038/msb.2011.75>
38
39 935 Skuzeski, J.M., Nichols, L.M., Gesteland, R.F., Atkins, J.F., 1991. The signal for a
40
41 936 leaky UAG stop codon in several plant viruses includes the two downstream
42
43 937 codons. *J. Mol. Biol.* 218, 365–373. [https://doi.org/10.1016/0022-2836\(91\)90718-L](https://doi.org/10.1016/0022-2836(91)90718-L)
44
45 938
46 939 Söding, J., Biegert, A., Lupas, A.N., 2005. The HHpred interactive server for protein
47
48 940 homology detection and structure prediction. *Nucleic Acids Res.* 33.
49
50 941 <https://doi.org/10.1093/nar/gki408>
51
52 942 Sola, I., Almazán, F., Zúñiga, S., Enjuanes, L., 2015. Continuous and Discontinuous
53
54 943 RNA Synthesis in Coronaviruses. *Annu. Rev. Virol.* 2, 265–288.
55
56 944 <https://doi.org/10.1146/annurev-virology-100114-055218>
57
58 945 te Velthuis, A.J.W., Arnold, J.J., Cameron, C.E., van den Worm, S.H.E., Snijder,
59
60 946 E.J., 2009. The RNA polymerase activity of SARS-coronavirus nsp12 is primer
61
62 947 dependent. *Nucleic Acids Res.* 38, 203–214. <https://doi.org/10.1093/nar/gkp904>
63
64
65

948 Tokarz, R., Sameroff, S., Hesse, R.A., Hause, B.M., Desai, A., Jain, K., Ian Lipkin,
1 W., 2015. Discovery of a novel nidovirus in cattle with respiratory disease. *J.*
2 Gen. Virol. 96, 2188–2193. <https://doi.org/10.1099/vir.0.000166>
3
4 Vasilakis, N., Guzman, H., Firth, C., Forrester, N.L., Widen, S.G., Wood, T.G., Rossi,
5 S.L., Ghedin, E., Popov, V., Blasdell, K.R., Walker, P.J., Tesh, R.B., 2014.
6 Mesoniviruses are mosquito-specific viruses with extensive geographic
7 distribution and host range. *Virol. J.* 11. <https://doi.org/10.1186/1743-422X-11-97>
8
9 Wahl-Jensen, V., Johnson, J.C., Lauck, M., Weinfurter, J.T., Moncla, L.H., Weiler,
10 A.M., Charlier, O., Rojas, O., Byrum, R., Ragland, D.R., Huzella, L., Zommer,
11 E., Cohen, M., Bernbaum, J.G., Caì, Y., Sanford, H.B., Mazur, S., Johnson,
12 R.F., Qin, J., Palacios, G.F., Bailey, A.L., Jahrling, P.B., Goldberg, T.L.,
13 O'Connor, D.H., Friedrich, T.C., Kuhn, J.H., 2016. Divergent simian arteriviruses
14 cause simian hemorrhagic fever of differing severities in macaques. *MBio* 7.
15 <https://doi.org/10.1128/mBio.02009-15>
16
17 Zeng, C., Wu, A., Wang, Y., Xu, S., Tang, Y., Jin, X., Wang, S., Qin, L., Sun, Y., Fan,
18 C., Snijder, E.J., Neuman, B.W., Chen, Y., Ahola, T., Guo, D., 2016.
19 Identification and Characterization of a Ribose 2'-O-Methyltransferase Encoded
20 by the Ronivirus Branch of Nidovirales. *J. Virol.* 90, 6675–6685.
21 <https://doi.org/10.1128/JVI.00658-16>
22
23 Zhao, L., Liu, L., Wang, S., Wang, H., Jiang, J., 2016. Transcriptome profiles of
24 metamorphosis in the ornamented pygmy frog *Microhyla fissipes* clarify the
25 functions of thyroid hormone receptors in metamorphosis. *Sci. Rep.* 6.
26 <https://doi.org/10.1038/srep27310>
27
28 Ziebuhr, J., Baric, R.S., Baker, S., de Groot, R.J., Drosten, C., Gulyaeva, A.,
29 Haagmans, B.L., Neuman, B.W., Perlman, S., Poon, L.L.M., Sola, I.,
30 Gorbatenya, A.E., 2017. ICTV Pending Proposal 2017.013S. Reorganization of
31 the family Coronaviridae into two families, Coronaviridae (including the current
32 subfamily Coronavirinae and the new subfamily Letovirinae) and the new family
33 Tobaniviridae (accommodating the current subf.
34
35 Zuker, M., 2003. Mfold web server for nucleic acid folding and hybridization
36 prediction. *Nucleic Acids Res.* 31, 3406–3415.
37 <https://doi.org/10.1093/nar/gkg595>
38
39
40
41
42
43
44
45
46
47
48
49
50
51
52
53
54
55
56
57
58
59
60
61
62
63
64
65

Figure 1

[Click here to download high resolution image](#)

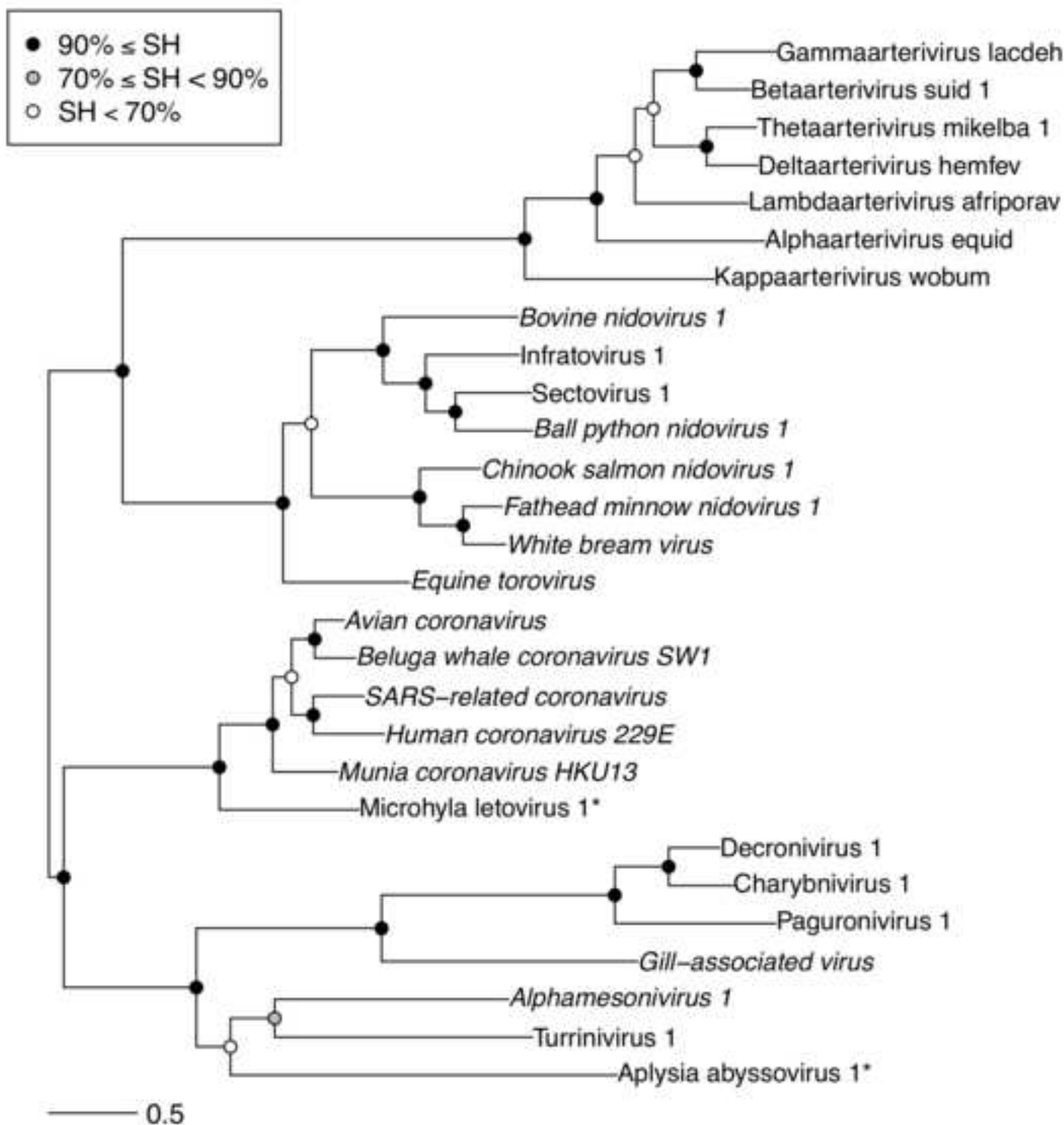


Figure 2

[Click here to download high resolution image](#)

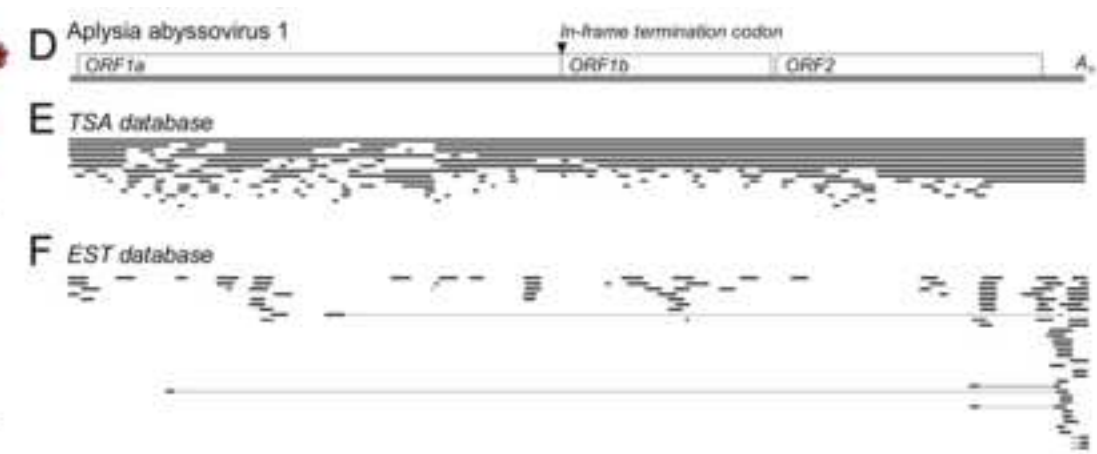
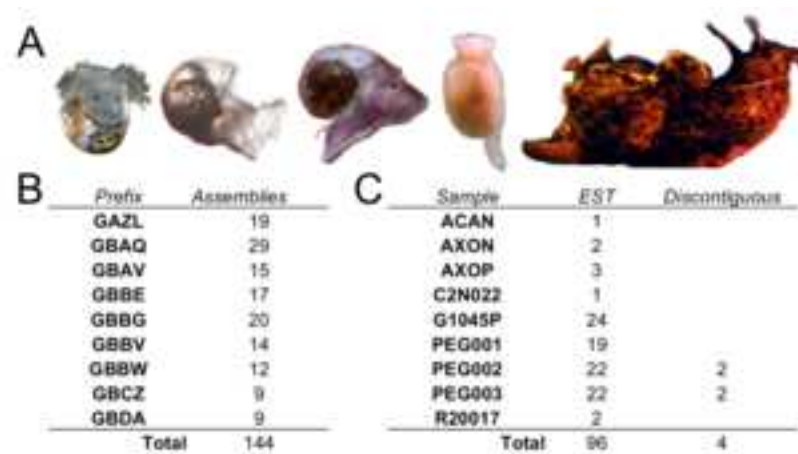
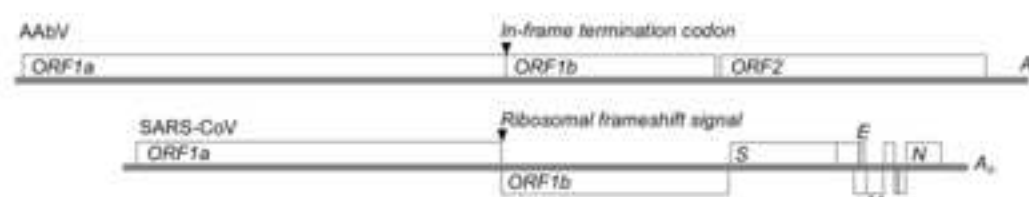


Figure 3

[Click here to download high resolution image](#)

A



C

5'-UTR 33-72 Possible TRS
 IGS 25212-51

D

Aplysia abyssovirus 1	Protein	Region	Input	Tool	Probability	E value	Model	Note
Main protease	pp1a	4401-4618	Abyssovirus 1 only	HHPred	96%	0.044	3D23	Main protease, Human coronavirus HKU1
Conserved pp1a	pp1a	5386-5629	Abyssovirus 1 only	Protein BLAST		1.0×10^{-7}	NC_032498	Unknown function, Turrivivirus 1
NIRAN	pp1ab	5953-6087	Abyssovirus 1 only	HHPred align	96%	9.4×10^{-8}	NP_828869	nsp12 NIRAN & RdRP, SARS-CoV
RNA dependent RNA polymerase	pp1ab	6497-6893	Abyssovirus 1 only	HHPred	99%	3.9×10^{-13}	2CKW	RNA dependent RNA polymerase, Sapporo virus
Metal binding helicase/NTPase	pp1ab	6963-7596	Abyssovirus 1 only	HHPred	100%	2.6×10^{-41}	5WWP	nsp13, Middle east respiratory syndrome-related-CoV
Exonuclease/N7 Methyltransferase	pp1ab	7628-7940	Alignment with Turrivivirus 1	HHPred	100%	1.4×10^{-89}	5C8T	nsp14 Exonuclease & N7 Methyltransferase, SARS-CoV
Exonuclease region	pp1ab	7655-7913	Abyssovirus 1 only	HHPred	87%	0.39	5C8T	nsp14 Exonuclease & N7 Methyltransferase, SARS-CoV
N7 Methyltransferase region	pp1ab	7891-8056	Abyssovirus 1 only	HHPred	32%	41	2P6J	SAM-dependent methyltransferase, Clostridium acetobutylicum
2O Methyltransferase	pp1ab	8248-8353	Abyssovirus 1 only	HHPred align	67%	3.2×10^{-4}	YP_001661452	nsp16 2'-O-methyltransferase, Gill-associated virus
Structural Protease	pp5	276-471	Abyssovirus 1 only	HHPred	99%	1.0×10^{-13}	2R0L	HGFA family S1 serine protease, Human

B

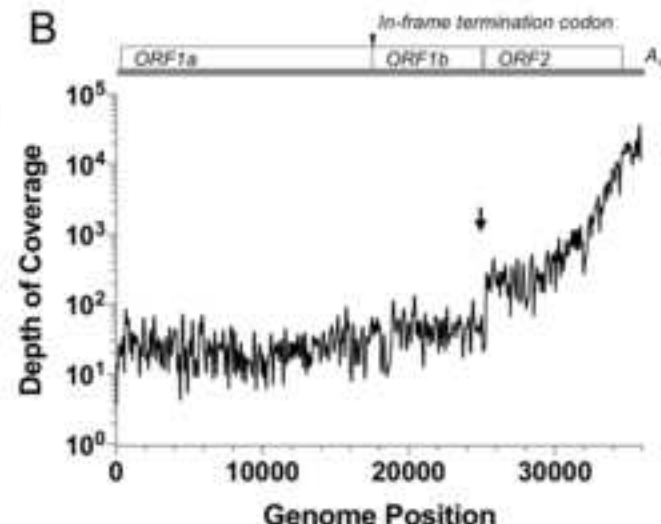


Figure 4

[Click here to download high resolution image](#)

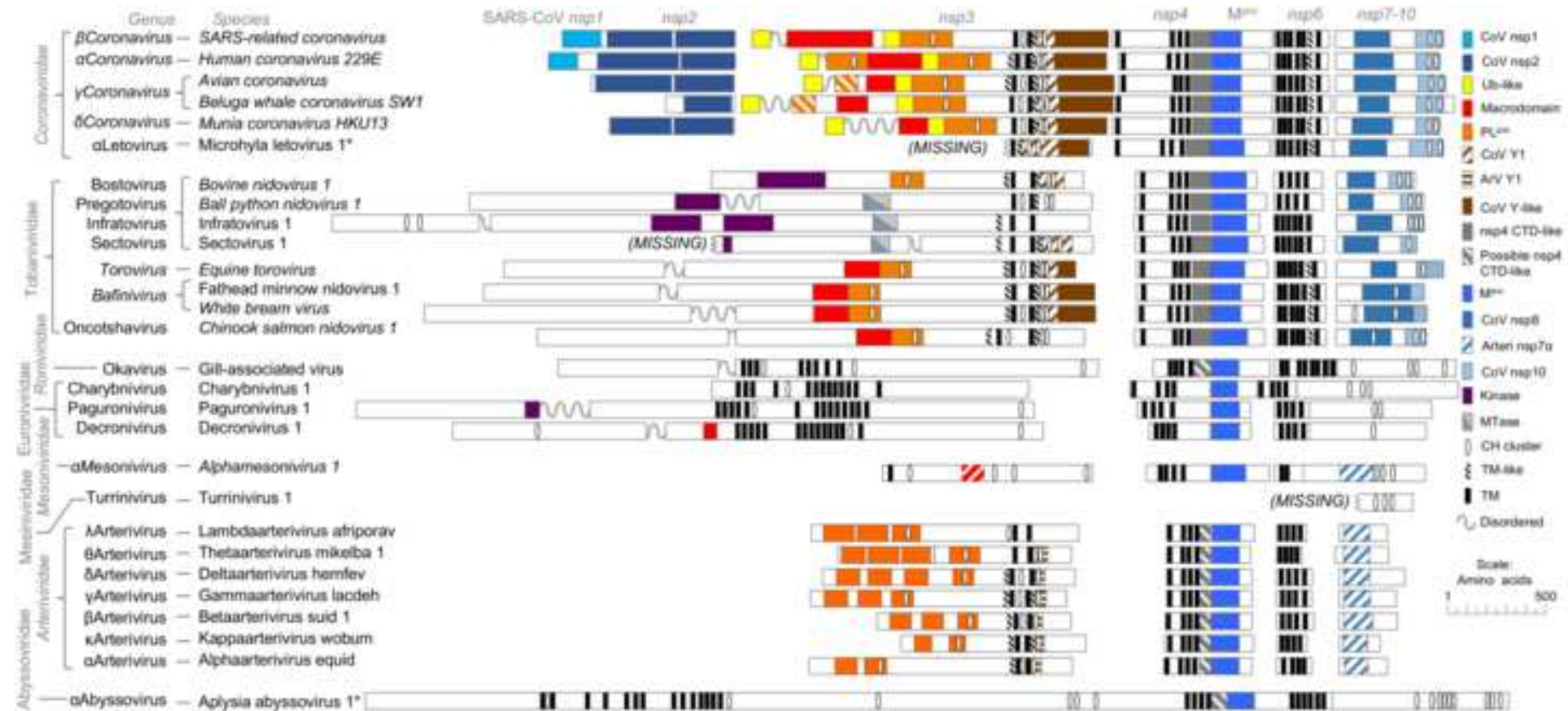
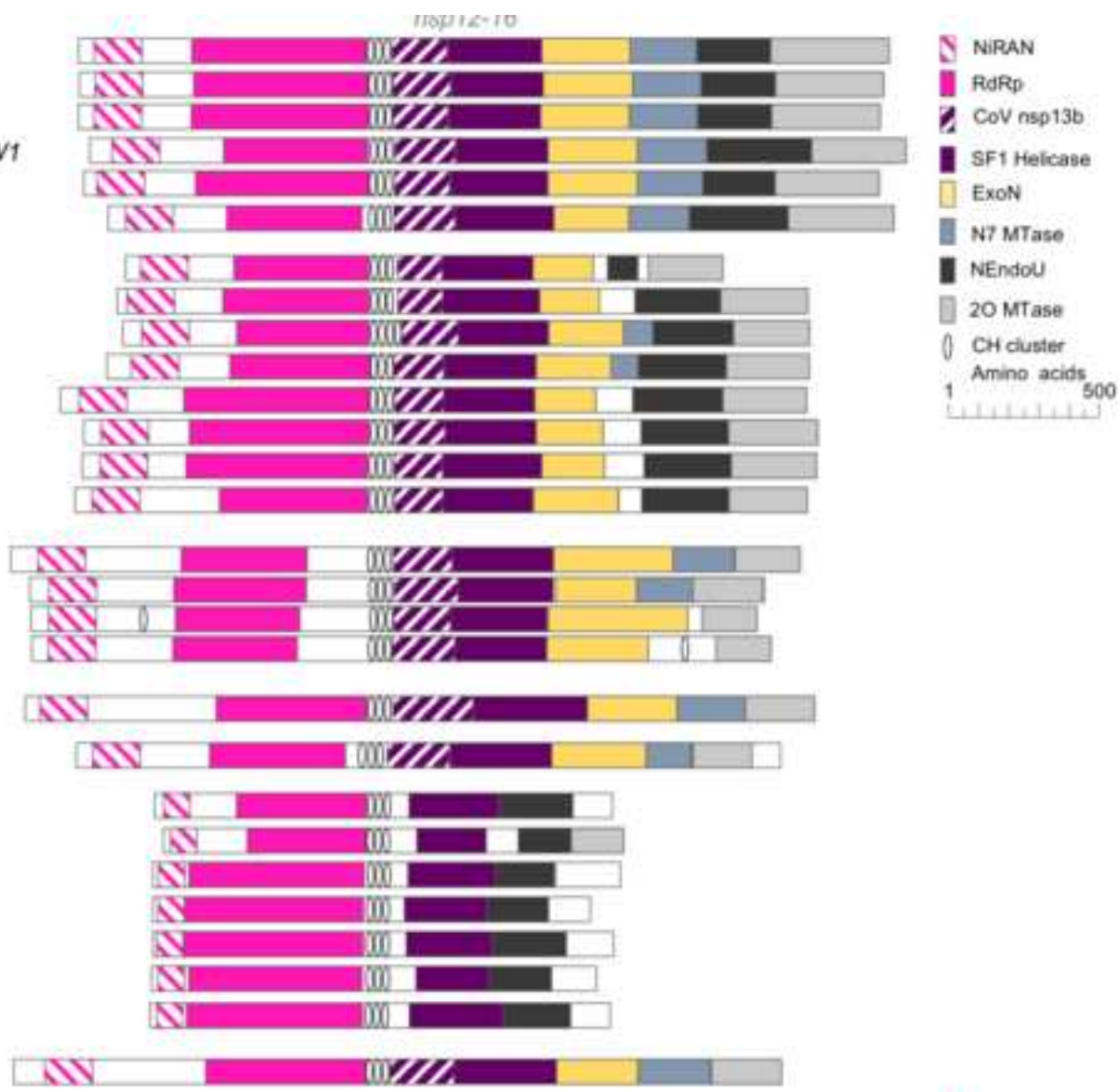


Figure 5

[Click here to download high resolution image](#)

A

	Genus	Species
Coronaviridae	β Coronavirus	SARS-related coronavirus
	α Coronavirus	Human coronavirus 229E
	γ Coronavirus	Avian coronavirus
		Beluga whale coronavirus SW1
	δ Coronavirus	Munia coronavirus HKU13
Tobaniviridae	α Letovirus	Microhyla letovirus 1*
	Bostovirus	Bovine nidovirus 1
	Pregotovirus	Ball python nidovirus 1
	Infratovirus	Infratovirus 1
	Sectovirus	Sectovirus 1
	Torovirus	Equine torovirus
	Bafinivirus	Fathead minnow nidovirus 1
		White bream virus
	Oncotshavirus	Chinook salmon nidovirus 1
	Euroniviridae	Okavirus
Charybnivivirus		Charybnivirus 1
Paguronivirus		Paguronivirus 1
Decronivirus		Decronivirus 1
α Mesonivivirus		Alphamesonivirus 1
Turrinivirus		Turrinivirus 1
λ Arterivirus		Lambdaarterivirus afriporav
θ Arterivirus		Thetaarterivirus mikelba 1
δ Arterivirus		Deltaarterivirus hemfev
γ Arterivirus		Gammaarterivirus lacdeh
β Arterivirus	Betaarterivirus suis 1	
κ Arterivirus	Kappaarterivirus wobum	
α Arterivirus	Alphaarterivirus equid	
α Abyssovirus	Aplysia abyssovirus 1*	



B

Aplysia abyssovirus 1* pp2



5'
Transmembrane
SignalP cleavage

Figure 6

[Click here to download high resolution image](#)

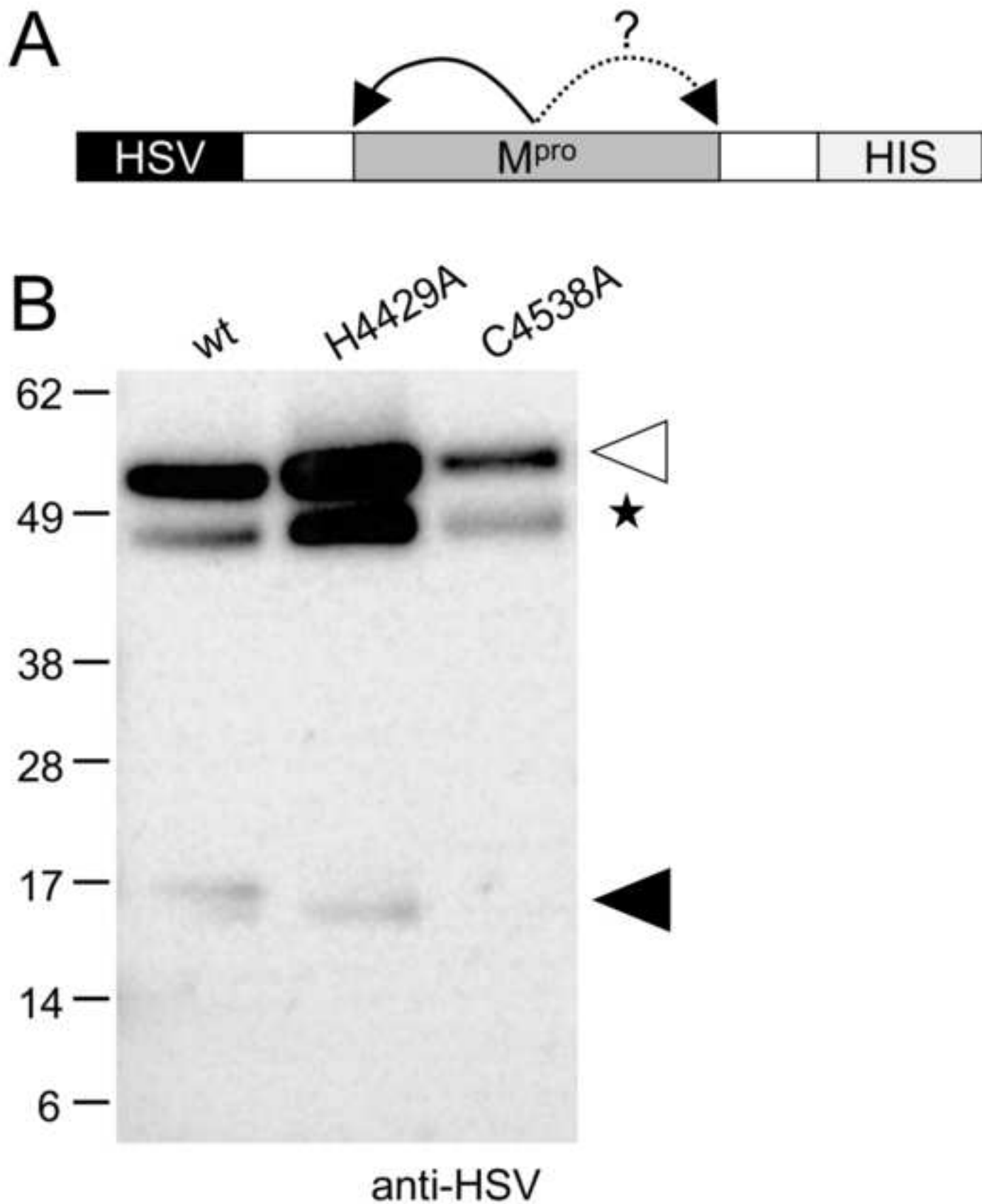


Figure 7

[Click here to download high resolution image](#)

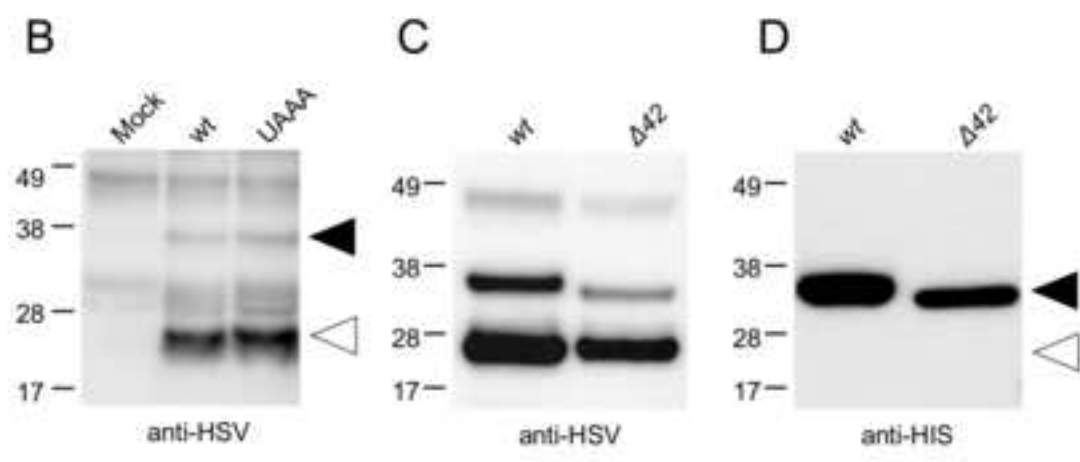
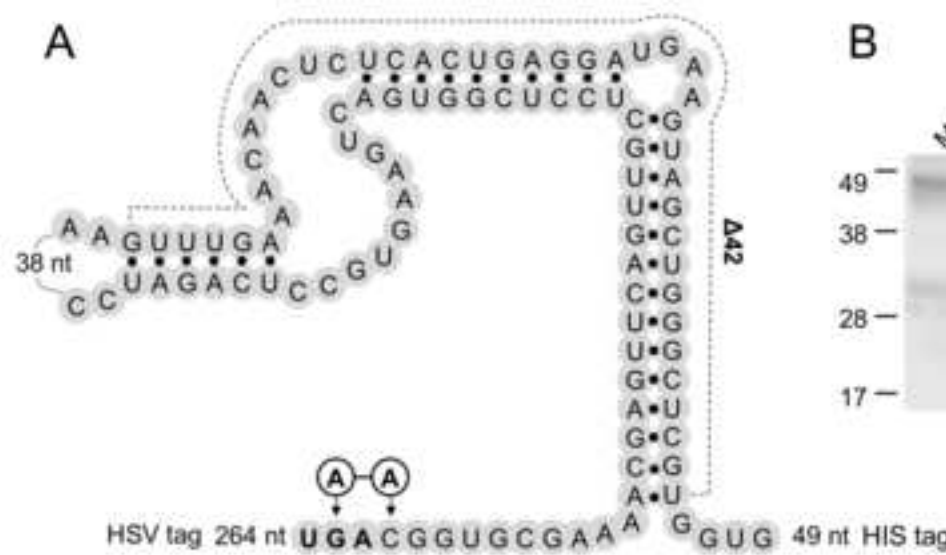
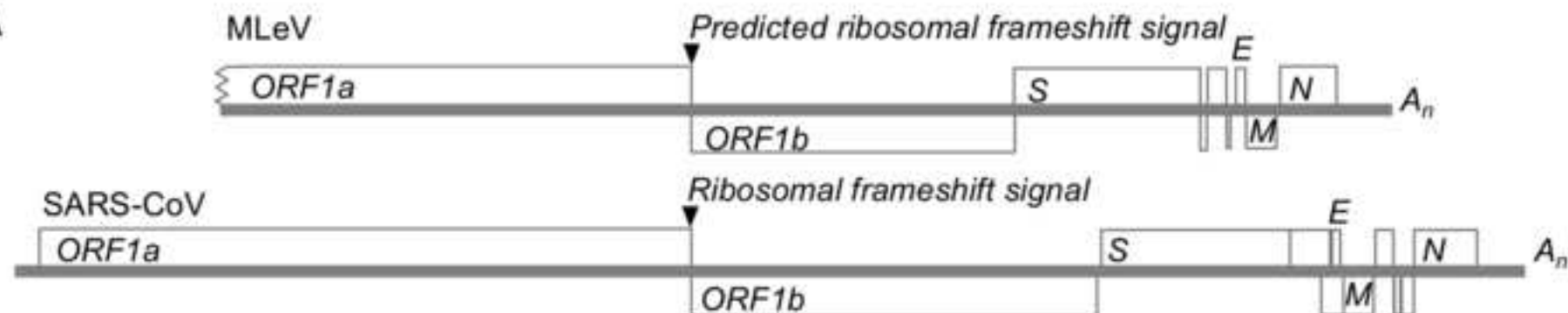


Figure 8

[Click here to download high resolution image](#)

A



B

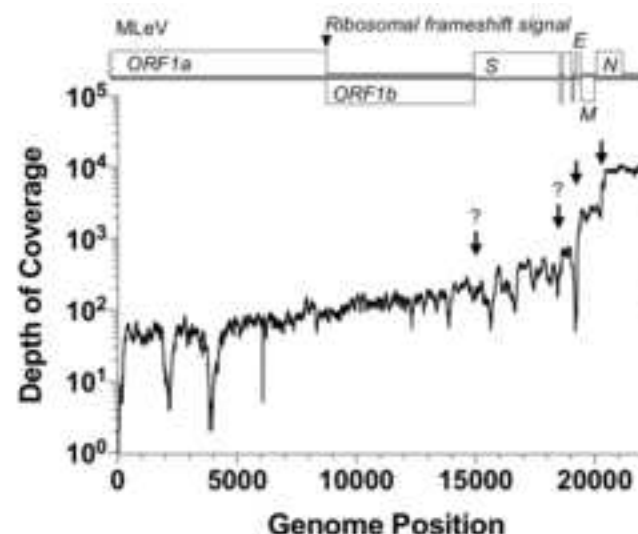


	Premetamorphosis	Metamorphic climax	Completion of metamorphosis
Read count	209301	32737	2298
FPKM	453.1	63.7	4.4

Figure 9

[Click here to download high resolution image](#)

A



B

Preceding Gene	Genome Position	Putative TRS?	Following Gene	Read Depth Increases	
pplb	13911	TTCAAC ATGA	S-like	no	
S-like <u>TAG</u> (40)	18538	TTCAATA	(55) ATG	ORF 3a	no
ORF 3b <u>TAA</u> (138)	19212	TTCAAAA	(48) ATG	E-like	yes
E-like	19439	TTCAATA ATG	M-like		
M-like <u>TAG</u> (41)	20272	TTCAAAA	(59) ATG	N-like	yes

C

Microfylavirus 1	Protein	Region	Input	Tool	Probability	E value	Model	Note
nsp3 Y domain	pp1a	104-287	MLeV only	HHPred align	96.6%	1.3×10^{-9}	NP_828862	nsp3 Y1 and CoV-Y domains, SARS-CoV
nsp4 N terminal region	pp1a	547-736	MLeV only	Protein BLAST		4.0×10^{-4}	APX44046	IBV nsp4
nsp4 C-terminal domain	pp1a	801-907	MLeV only	HHPred	100%	3.8×10^{-37}	3VC8	FCoV nsp4 C-terminal domain
nsp5 M==	pp1a	924-1211	MLeV only	HHPred	100%	3.0×10^{-19}	3D23	HCoV-HKU1 M==
nsp6	pp1a		MLeV only	Protein BLAST		4.0×10^{-2}	APD51497	229E-related bat CoV nsp6
nsp7	pp1a	1508-1597	MLeV only	HHPred	99.9%	3.1×10^{-29}	1YSY	SARS-CoV nsp7
nsp8	pp1a	1598-1783	MLeV only	HHPred	100%	3.7×10^{-71}	3UB0	FCoV nsp8
nsp9	pp1a	1784-1894	MLeV only	HHPred	99.9%	3.1×10^{-39}	2,98	HCoV-229E nsp9
nsp10	pp1a	1901-2021	MLeV only	HHPred	100%	1.0×10^{-4}	5C8S	SARS-CoV nsp10
nsp12 NIRAN	pp1ab	2105-2252	MLeV only	Protein BLAST		3.0×10^{-13}	YP_005352845	NIRAN, Sparrow CoV HKU17
nsp12 middle domain	pp1ab	2285-2445	MLeV only	HHPred	97.4%	8.9×10^{-6}	4S1T	Fragmentary second NEndoU, HCoV-229E
nsp12 RdRp	pp1ab	2461-2909	MLeV only	HHPred	99.5%	3.5×10^{-17}	2CJO	BVDV RdRp
nsp13 ZF/Helicase	pp1ab	2954-3549	MLeV only	HHPred	99.9%	9.4×10^{-32}	4N0N	EAV nsp10 ZF/Helicase
nsp14 ExoN/N7-Methyltransferase	pp1ab	3568-4009	MLeV only	HHPred	100%	4.0×10^{-100}	5C8S	SARS-CoV nsp14
nsp15 NEndoU	pp1ab	4010-4327	MLeV only	HHPred	100%	2.4×10^{-64}	2GTI	MHV nsp15
nsp16 2O-Methyltransferase	pp1ab	4328-4631	MLeV only	HHPred	100%	4.8×10^{-41}	2XYQ	SARS-CoV nsp16
Putative Spike homolog	S	1-1526	MLeV only	TMHMM 2.0, SignalP 4.1, PSIPRED 3.3	n/a	n/a		Signal peptidase cleavage, N-terminal beta region, C-terminal alpha region, 1 TM predicted – S-like by inference
Putative E protein homolog	E	1-77	MLeV only	TMHMM 2.0, Amphiphaseek	n/a	n/a		1 TM, amphipathic region – E-like by inference
Membrane protein	M	1-130	MLeV only	Protein BLAST	88.5%	0.36	ADX59454	MERS-CoV N protein N-terminal domain
Nucleoprotein N-terminal domain	N	8-133	MLeV only	HHPred		0.4	4UD1	Cardioderma bat CoV Kenya/KY43/2006 M

Figure 10

[Click here to download high resolution image](#)

